

Quasi-relativistic approach to analytical gradients of parity violating potentials^{a)}

Sascha A Brück,¹ Nityananda Sahu,² Konstantin Gaul,² and Robert Berger^{1,2,3}

¹⁾Frankfurt Institute for Advanced Studies, Ruth-Moufang-Straße 1, 60438 Frankfurt am Main, Germany

²⁾Fachbereich Chemie, Philipps-Universität Marburg, Hans-Meerwein-Straße 4, 35032 Marburg, Germany

³⁾Clemens-Schöpf-Institut, Technische Universität Darmstadt, Alarich-Weiss-Straße 4, 64287, Darmstadt, Germany

(Dated: 14 December 2022)

An analytic gradient approach for the computation of derivatives of parity-violating (PV) potentials with respect to displacements of the nuclei in chiral molecules is described and implemented within a quasirelativistic mean-field framework. Calculated PV potential gradients are utilised for estimating PV frequency splittings between enantiomers in rotational and vibrational spectra of four chiral polyhalomethanes, i.e. CHBrClF, CHClFI, CHBrFI and CHAtFI. Values calculated within the single-mode approximation for the frequency shifts agree well with previously reported theoretical values. The influence of non-separable anharmonic effects (multi-mode effects) on the vibrational frequency shifts, which are readily accessible with the present analytic derivative approach, are estimated for the C–F stretching fundamental of all four molecules and computed for each of the fundamentals in CHBrClF and CHAtFI. Multi-mode effects are found to be significant, in particular for the C–F stretching modes, being for some modes and cases of similar size as the single-mode contribution.

I. INTRODUCTION

Early after the proof of parity violation (PV) was provided in 1957 by the famous experiment of β^- disintegration of Co nuclei¹, which realised a proposal by the theoreticians Lee and Yang², it was suggested by Yamagata³ that PV weak interactions can induce a tiny energy difference between a chiral molecule and its non-identical mirror-image.^{4–12} Diverse experimental schemes have been proposed to detect PV effects in chiral molecules, ranging from Mössbauer spectroscopy¹³ to vibrational spectroscopy,^{14–17} electron paramagnetic resonance spectroscopy,¹⁸ rotational spectroscopy^{16,19} and nuclear magnetic resonance spectroscopy^{20–23} to time-dependent approaches and quantum-beat experiments^{12,24–26}. We refer the reader for more details and an extended overview to a collections of reviews on this subject^{27–33}. The most accurate experimental attempts reported so far were in the high-resolution infrared spectroscopy of bromochlorofluoromethane (CHBrClF). An upper bound of $\Delta v_{\text{PV}}/v \approx 10^{-13}$ was obtained for the relative PV difference of the C–F stretching frequency between (*R*)- and (*S*)-enantiomers.¹⁷ The theoretically^{34–41} predicted value for this relative frequency splitting is of the order of 10^{-17} , however. Later, with an improved experimental set-up, a measurement of the same compound with a resolution of 5×10^{-14} has been reported in 2002⁴² and with a new set-up, it may be hoped that a precision of 10^{-16} can be reached.^{43,44} As nuclear spin-independent electroweak PV effects in chiral compounds scale approximately with nuclear charge *Z* to the power of five (in the presence of spin-orbit coupling), compounds containing heavy metal nuclei could be of greater experimental value than the

originally used organic molecules. Theoretical searches in this direction have been already made on molecules containing for instance bismuth, rhenium, mercury and astatine.^{40,45–47}

In general, a measurement of the PV energy as a difference between electronic energies of separated enantiomers would be very difficult since it comes on top of the rest mass energy of the molecule,⁵ but the scheme proposed by Quack¹², for instance, circumvents this by directly measuring the PV energy via the PV induced time-dependent interconversion between states of opposite parity²⁷. An alternative for detecting molecular parity violation is to measure the difference between PV energy differences arising due to the PV potential $[E_{\text{PV}}(\vec{q})]$ in the vibrational and rotational transitions in chiral compounds,⁵ with \vec{q} denoting the vector of dimensionless reduced normal coordinates. Often also V_{PV} is used as symbol for the PV potential. In first order perturbation theory, $E_{\text{PV}}(\vec{q})$ gives rise to a PV shift in the *n*th vibrational energy level of a given enantiomer (*R* or *S*) according to³⁷

$$E_{n,\text{PV}}^{R,S} \approx \langle \Psi_n^{R,S} | E_{\text{PV}}(\vec{q}) | \Psi_n^{R,S} \rangle, \quad (1)$$

where $|\Psi_n^{R,S}\rangle$ denote the *n*th vibrational state of the *R*- and *S*-enantiomer, which are obtained by solving the parity-conserving (PC) rovibrational Schrödinger equation for each enantiomer. Since, $E_{\text{PV}}(\vec{q})$ is parity odd, $E_{n,\text{PV}}^R$ and $E_{n,\text{PV}}^S$ values are numerically of equal magnitude but have an opposite sign. Thus, the corresponding PV energy difference between the *n*th vibrational levels of the two enantiomers is

$$\Delta E_{n,\text{PV}} = E_{n,\text{PV}}^S - E_{n,\text{PV}}^R \approx 2 \langle \Psi_n^S | E_{\text{PV}}(\vec{q}) | \Psi_n^S \rangle. \quad (2)$$

The relative change in vibrational ($\Delta E_{\text{vib,PV}} = \Delta E_{m,\text{PV}} - \Delta E_{n,\text{PV}}$) and rotational ($\Delta E_{\text{rot,PV}}$) transition energies between right- and left-handed molecules is expected to scale to same order of magnitude as that of the relative change in electronic

^{a)}Parts of this work were reported in preliminary form in S. Brück, Diploma thesis, University of Frankfurt, 2011.

($\Delta E_{\text{el,PV}}$) transition energy.⁴⁸

$$\frac{\Delta E_{\text{el,PV}}}{E_{\text{el}}} \approx \frac{\Delta E_{\text{vib,PV}}}{E_{\text{vib}}} \approx \frac{\Delta E_{\text{rot,PV}}}{E_{\text{rot}}} \quad (3)$$

The introduction of PV within electroweak quantum chemistry not only affects the energy of an enantiomer, but also its equilibrium structure if the PC vibrational potential gets modified by the PV potential.³⁷ In general, the PV potential induces a minute change in the equilibrium structure of a molecule compared to the equilibrium structure without PV contribution, if the PV energy gradient ($\vec{\nabla}E_{\text{PV}}$) does not vanish there. Thus, the weak interaction leads to a change of the equilibrium structure of a chiral molecule, which is different for both enantiomers due to PV effects.

This effect could in principle be measured by microwave spectroscopy, since it leads to a shift of the rotational constants.³⁴ In practice, the change of the structure due to $\vec{\nabla}E_{\text{PV}}$ at the minimum of the parity conserving potential can be estimated with the help of the vibrational Hessian \mathbf{F}_{MW} ,³⁷ of the PC potential, given in mass-weighted Cartesian displacement coordinates. From this $3N_{\text{nuc}} \times 3N_{\text{nuc}}$ -dimensional vibrational Hessian, with N_{nuc} being the number of nuclei in the system, contributions of infinitesimal translational and rotational displacements can be eliminated with the $3N_{\text{nuc}} \times (3N_{\text{nuc}} - 6)$ dimensional projection matrix \mathbf{A} by forming $(\mathbf{A}^T \mathbf{F}_{\text{MW}} \mathbf{A})^{-1}$, so that the corresponding Hessian in internal Cartesian displacement coordinates results, which can be inverted. When \mathbf{M} is a $(3N_{\text{nuc}} \times 3N_{\text{nuc}})$ diagonal matrix containing the masses of the various atoms, the final displacements ($\delta_{\text{PV}} \vec{R}$) of the atoms from their equilibrium position due to $\vec{\nabla}E_{\text{PV}}$ read

$$\delta_{\text{PV}} \vec{R} = -\mathbf{M}^{-1/2} \mathbf{A} (\mathbf{A}^T \mathbf{F}_{\text{MW}} \mathbf{A})^{-1} \mathbf{A}^T \mathbf{M}^{-1/2} \vec{\nabla} E_{\text{PV}}. \quad (4)$$

Coordinates and displacements are transformed subsequently to the principal axis system of the PC equilibrium structure and the splittings of the diagonal elements ($\Delta \mathbf{I}$) of the moment of inertia tensor due to PV effects are approximated to first order in $\delta_{\text{PV}} \vec{R}$. For the xx component of $\Delta \mathbf{I}$ we have for instance:

$$\Delta I_x = 2m_A (y_A \delta_{\text{PV}} y_A + z_A \delta_{\text{PV}} z_A) \quad (5)$$

and analogous for the other diagonal elements. Then, the changes in diagonal elements are used to estimate the splittings of rotational constants (ΔX_{R}) between two enantiomers within the approximate expression³⁷

$$\frac{\Delta X_{\text{R}}}{X_{\text{R}}} \approx -\frac{\Delta I_X}{I_X} \quad (6)$$

with X_{R} being one of the rotational constants (A , B or C) and I_X being the corresponding eigenvalues of the moment of inertia tensor. From Eq. 4 the importance of the gradient of the parity violating potential with respect to displacements of the nuclei becomes particularly evident. The numerical calculation of this term, however, is tedious, in particular within a (quasi)relativistic electronic structure framework, which is why we present in this work an approach for calculating this gradient analytically within a quasirelativistic mean-field framework.

Another promising experiment for detecting parity violation in chiral molecules is vibrational spectroscopy. Most of the effort has been put into the measurement of vibrational frequency shifts due to PV effects.^{14,16,17,34,36,38,40,42,49-52} The relative vibrational frequency shift for a transition from state n to m is determined by taking the difference of the vibrationally averaged PV potentials of the enantiomers and dividing by the corresponding transition energy $h\nu_{mn}$ ^{37,40}

$$\frac{\Delta \nu_{mn,\text{PV}}}{\nu_{mn}} = 2 \frac{(\langle \Psi_m | E_{\text{PV}}(\vec{q}) | \Psi_m \rangle - \langle \Psi_n | E_{\text{PV}}(\vec{q}) | \Psi_n \rangle)}{h\nu_{mn}} \quad (7)$$

where the factor two enters into the equation since the difference of the R and S enantiomer is twice (*cf.* Eq. 2) the difference between one enantiomer and the parity conserving case, where no shift occurs.⁴⁰ The vibrationally averaged potentials depend on the multi-dimensional PV energy surface and not only on a single point energy at the equilibrium structure. In addition, the complete rovibrational wavefunction would be needed to compute the expectation value. As this problem is extremely complex even for relatively small molecules, the PV effects of electronic, vibrational and rotational degrees of freedom are typically separated in a first step. Still the computational effort is in general too high, so as a second step, the multi-dimensional problem is usually split into one-dimensional problems, where the movements along the normal coordinates are treated separately as if they were independent of each other.^{37,40} This can be augmented by adding contributions from the potential depending on a smaller number of modes order by order.^{53,54} In practice, the PC potential (V_{BO}) and PV potential [$E_{\text{PV}}(\vec{q})$] can be evaluated at one-dimensional cuts along the dimensionless reduced normal coordinates \vec{q} .^{37,40} This approach has already been used to estimate the vibrational frequency splitting of the C-F stretching mode in chiral halogenated methane derivatives.^{34,35,37,38,40,52}

A different approach comes from perturbation theory,⁵⁵ where the PC and PV potentials are expanded in a Taylor series. In this, the influence of multi-mode effects are estimated by the calculations of the derivatives of the PV potentials with respect to all normal coordinates. The contributions of lowest non-vanishing order to the n^{th} vibrational energy levels of a normal mode ν_r within the perturbative treatment are

$$\begin{aligned} \langle \Psi_{n_r} | E_{\text{PV}}(\vec{q}) | \Psi_{n_r} \rangle &\approx E_{\text{PV}}(\vec{R}_0) \\ &+ \frac{1}{2} \left(n_r + \frac{1}{2} \right) \left(\frac{\partial^2 E_{\text{PV}}}{\partial q_r^2} - \sum_s \frac{1}{\hbar \omega_s} \frac{\partial^3 V_{\text{BO}}}{\partial q_r^2 \partial q_s} \frac{\partial E_{\text{PV}}}{\partial q_s} \right) \end{aligned} \quad (8)$$

where $E_{\text{PV}}(\vec{R}_0)$ is the PV energy at the equilibrium structure and ω_s denotes the harmonic vibrational angular frequency of normal mode ν_s . The terms $\frac{\partial E_{\text{PV}}}{\partial q_s}$ and $\frac{\partial^2 E_{\text{PV}}}{\partial q_r^2}$ are the first (gradient) and second partial derivatives of the PV energy along normal coordinates (q_s , q_r), respectively. Ignoring all the $r \neq s$ terms in the second sum of Eq. 8 gives the one-dimensional (1D) perturbative estimate of the vibrational energy for normal mode ν_r as

$$\begin{aligned} \langle \Psi_{n_r} | E_{\text{PV}}(q_r) | \Psi_{n_r} \rangle^{\text{1D}} &= E_{\text{PV}}(\vec{R}_0) \\ &+ \frac{1}{2} \left(n_r + \frac{1}{2} \right) \left(\frac{\partial^2 E_{\text{PV}}}{\partial q_r^2} - \frac{1}{\hbar \omega_r} \frac{\partial^3 V_{\text{BO}}}{\partial q_r^3} \frac{\partial E_{\text{PV}}}{\partial q_r} \right). \end{aligned} \quad (9)$$

The drawback of this method is that the one-dimensional terms of the PC and PV potentials are not included to infinite order. But the advantage is that, once the Cartesian gradient of the PV energy at the equilibrium structure is known, the two-dimensional coupling term can be included without too much effort, because only the semidiagonal cubic force constants are needed, whereas the gradient of PV energy along all the normal mode can conveniently be determined by projecting the Cartesian PV energy gradient onto displacements along to the normal coordinates. Hence, contributions from other modes (*cf.* Eq. 10) in addition to the single-mode terms described by Eq. 9 can easily be accounted for by considering first order multi-mode (MM) effects on the vibrational energy levels as shown in Eq. 8

$$\langle \Psi_{n_r} | E_{\text{PV}}(\vec{q}) | \Psi_{n_r} \rangle^{\text{MM}} = -\frac{1}{2} \left(n_r + \frac{1}{2} \right) \sum_{s \neq r} \frac{1}{\hbar \omega_s} \frac{\partial^3 V_{\text{BO}}}{\partial q_r^2 \partial q_s} \frac{\partial E_{\text{PV}}}{\partial q_s}. \quad (10)$$

We define with these MM terms the perturbative approximation of the vibrational energy shifts with 2D coupling terms as

$$\langle \Psi_{n_r} | E_{\text{PV}}(\vec{q}) | \Psi_{n_r} \rangle^{2\text{D}} = \langle \Psi_{n_r} | E_{\text{PV}}(\vec{q}) | \Psi_{n_r} \rangle^{1\text{D}} + \langle \Psi_{n_r} | E_{\text{PV}}(\vec{q}) | \Psi_{n_r} \rangle^{\text{MM}}. \quad (11)$$

Thus, for the calculation of the influence of PV on the vibrational and rotational spectra, which is one of the main goals of the current manuscript, the knowledge of the gradient of the PV potential along all the normal modes is essential. The present article describes an analytical approach for calculating the gradient of the PV energy ($\vec{\nabla} E_{\text{PV}}$) at HF and LDA level of theory (see the following section II). These values obtained from this analytic gradient approach, with corresponding computational details being described in section III, are then utilised in section IV for determining the relative shifts in rotational constants and vibrational frequencies, due to PV effects in chiral methane derivatives. Besides this, the influence of non-separable anharmonic effects (multi-mode effects) on PV induced vibrational frequency shifts for all the vibrational normal modes is calculated for CHBrCIF and CHAtFI molecules.

II. THEORY

For the description of the vibrational movement of nuclei in the Born-Oppenheimer approximation, it is often sufficient to evaluate the electronic structure for a single fixed arrangement of the nuclei described by the coordinates \vec{R}_0 and to treat the displacement of nuclei perturbatively (see also Refs. 56–58).

The electroweak parity-violating potential is very small compared to the PC potential due to the appearance of the Fermi coupling constant which is $2.22249 \times 10^{-14} E_{\text{h}} a_0^3$ in atomic units. Therefore, we can treat the parity-violating electroweak Hamiltonian \hat{H}_{PV} as a small addition to the parity conserving molecular Hamiltonian \hat{H}_0 :

$$\hat{H} = \hat{H}_0 + \lambda_{\text{PV}} \hat{H}_{\text{PV}}, \quad (12)$$

where we have introduced λ_{PV} as a formal perturbation parameter.

In a mean-field approach the leading order parity violating contribution $E_{\text{PV}}(\vec{R}_0 + \vec{\eta}, \lambda_{\text{PV}}) = E(\vec{R}_0 + \vec{\eta}, \lambda_{\text{PV}}) - E(\vec{R}_0)$ to the gradient of the variational energy with respect to nuclear displacements is:

$$\vec{\nabla}_{\vec{\eta}} E_{\text{PV}}(\vec{R}_0 + \vec{\eta}, \lambda_{\text{PV}}) \Big|_{\vec{\eta}=\vec{0}} \approx \lambda_{\text{PV}} \frac{\partial \vec{\nabla}_{\vec{\eta}} E(\vec{R}_0 + \vec{\eta}, \lambda_{\text{PV}})}{\partial \lambda_{\text{PV}}} \Big|_{\substack{\vec{\eta}=\vec{0} \\ \lambda_{\text{PV}}=0}} \quad (13)$$

For details on the specific case of electroweak parity violation, see Appendix A, whereas for the general case of variational perturbation theory, see e.g. Ref. 59.

In this paper, we want to focus on the molecular Hamiltonian approximated within a (quasi-relativistic) two-component zeroth-order regular approximation (ZORA) framework^{60,61} on the level of Generalised Hartree-Fock (GHF) or Generalised Kohn-Sham (GKS) density functional theory (DFT) (see Ref. 62 and 63):

$$\hat{H}_0 = \hat{H}_{\text{ZORA}} = \mathbf{V}_{\text{GHF,GKS}} + \underbrace{\hat{V}_{\text{nuc}}(\vec{r}) + c^2 \vec{\sigma} \cdot \hat{p} \omega(\vec{r}) \vec{\sigma} \cdot \hat{p}}_{\hat{h}_{\text{ZORA}}} \quad (14)$$

Here, $\mathbf{V}_{\text{GHF,GKS}}$ is the effective electron repulsion potential within the GHF or GKS framework, \hat{p} is the linear momentum operator, $\vec{\sigma}$ is the vector of Pauli spin matrices and $\omega(\vec{r}) = \frac{1}{2c^2 - \tilde{V}(\vec{r})}$ is the ZORA factor with the ZORA model potential \tilde{V} as proposed by van Wüllen to alleviate the gauge dependence of ZORA.⁶² The ZORA one-electron operator has an electron spin-independent and an electron spin-dependent contribution:

$$\hat{h}_{\text{ZORA}} = \hat{V}_{\text{nuc}} + \underbrace{c^2 \hat{p} \cdot \left(\omega(\vec{r}) \hat{p} \right)}_{\hat{h}_{\text{ZORA}}^{(0)}} + \underbrace{c^2 i \hat{p} \times \left(\omega(\vec{r}) \hat{p} \right) \cdot \vec{\sigma}}_{\hat{h}_{\text{ZORA}}^{(1,2,3)}} \quad (15)$$

Within ZORA, the nuclear-spin independent parity-violating electroweak one-electron Hamiltonian appears as⁶⁴

$$\hat{h}_{\text{PV}} = \frac{G_{\text{F}}}{2\sqrt{2}} \underbrace{\sum_{A=1}^{N_{\text{nuc}}} \left\{ \omega(\vec{r}) Q_{\text{W,A}} \rho_{\text{A}}(\vec{r}), c \hat{p} \right\}_+}_{\hat{h}_{\text{PV}}^{(1,2,3)}} \cdot \vec{\sigma}, \quad (16)$$

where $\{A, B\}_+ = AB + BA$ is the anti-commutator, $Q_{\text{W,A}}$ is the weak charge of nucleus A and ρ_{A} is the normalised nuclear density distribution. This operator has only electron spin-dependent contributions.

We expand the ZORA two-component HF or KS molecular orbitals (MOs) ϕ_i in a linear combination of real one-component basis functions χ_{μ} and complex two-component

coefficients $\vec{C}_{\mu i} = \begin{pmatrix} C_{\mu i}^{(\alpha)} \\ C_{\mu i}^{(\beta)} \end{pmatrix}$ as

$$\phi_i = \sum_{\mu} \vec{C}_{\mu i} \chi_{\mu} \quad (17)$$

In this two-component framework, we can define four complex one-component density matrices ($\kappa = 0, 1, 2, 3$):

$$D_{\mu\nu}^{(\kappa)} = \sum_{i=1}^{N_{\text{orb}}} n_i \underbrace{\bar{C}_{\mu i}^\dagger \sigma^\kappa C_{\nu i}}_{D_{i\mu\nu}^{(\kappa)}}, \quad (18)$$

where the 0th component of the Pauli spin matrices is the 2×2 identity matrix. The two-component density matrix can be written in terms of these one-component density matrices as

$$\mathbf{D} = \frac{1}{2} \sum_{\kappa=0}^3 (\sigma^\kappa)^* \otimes \mathbf{D}^{(\kappa)}. \quad (19)$$

We can write the expectation value of the one electron

ZORA operator as

$$h_{\text{ZORA}} = \sum_{\mu\nu} \Re \left\{ \sum_{\kappa=0}^3 D_{\mu\nu}^{(\kappa)} h_{\text{ZORA},\mu\nu}^{(\kappa)} \right\}, \quad (20)$$

and the energy contribution of the parity-violating electroweak potential as

$$h_{\text{PV}} = \sum_{\mu\nu} \Re \left\{ \sum_{\kappa=1}^3 D_{\mu\nu}^{(\kappa)} h_{\text{PV},\mu\nu}^{(\kappa)} \right\}. \quad (21)$$

In the following, the effective potential $\mathbf{V}_{\text{GHF,GKS}}$ will be represented in the space of basis functions in terms of the matrix of contracted two-electron integrals \mathbf{G} . In the general case of hybrid DFT, $\mathbf{G}^{(\kappa)}$ is constructed as

$$G_{\mu\nu}^{(\kappa)}(\mathbf{D}) = \sum_{\rho\sigma} \left[\delta_{\kappa 0} D_{\rho\sigma}^{(\kappa)}(\mu\nu|\rho\sigma) - a_X \frac{1}{2} D_{\rho\sigma}^{(\kappa)}(\mu\sigma|\rho\nu) + a_{\text{DFT}} \langle \chi_\mu | V_{\text{XC}}^{(\kappa)}(\mathbf{D}) | \chi_\nu \rangle \right], \quad (22)$$

where the Mulliken notation for two electron integrals is employed: $(\mu\nu|\rho\sigma) = \iint d^3r_1 d^3r_2 \chi_\mu(\vec{r}_1) \chi_\rho(\vec{r}_2) \frac{1}{|\vec{r}_1 - \vec{r}_2|} \chi_\nu(\vec{r}_1) \chi_\sigma(\vec{r}_2)$. In case of pure DFT (non-hybrid) we have $a_X = 0$ and in case of pure HF we have $a_X = 1$ and $a_{\text{DFT}} = 0$.

We consider non-relativistic density functionals which do not depend on the current density, which are commonly employed even in relativistic electronic structure theory. In this case, the matrix elements of the exchange-correlation potential $\langle \chi_\mu | V_{\text{XC}}^{(\kappa)} | \chi_\nu \rangle$ are always real. In this paper, we restrict the discussion to the spin-unpolarised local density approximation (LDA), in which the exchange-correlation potential has the form

$$V_{\text{XC,LDA}}^{(0)} = \frac{\delta F_{\text{XC,LDA}}[\rho_e(\vec{r}; \mathbf{D}^{(0)})]}{\delta \rho_e(\vec{r}; \mathbf{D}^{(0)})}, \quad (23)$$

with $F_{\text{XC,LDA}}$ being the LDA density functional and the electronic number density function being

$$\rho_e(\vec{r}; \mathbf{D}^{(0)}) = \sum_{\mu\nu} \Re \left\{ D_{\mu\nu}^{(0)} \right\} \chi_\mu(\vec{r}) \chi_\nu(\vec{r}). \quad (24)$$

For the general form of the exchange-correlation potential see Appendix B.

The expectation value of the electron repulsion potential is

$$V_{\text{GHF,GKS}} = \Re \left\{ \sum_{\kappa=0}^3 D_{\mu\nu}^{(\kappa)} G_{\mu\nu}^{(\kappa)}(\mathbf{D}) \right\}. \quad (25)$$

The total ZORA energy in presence of the full perturbation \hat{H}_{PV} , which implies $\lambda_{\text{PV}} = 1$, is given by

$$\begin{aligned} E_\infty &= h_{\text{ZORA}} + \frac{1}{2} V_{\text{GHF,GKS}} + h_{\text{PV}} \\ &= \Re \left\{ \sum_{\mu\nu} \left[\sum_{\kappa=0}^3 D_{\mu\nu}^{\infty,(\kappa)} h_{\text{ZORA},\mu\nu}^{(\kappa)} + \frac{1}{2} \sum_{\kappa=0}^3 D_{\mu\nu}^{\infty,(\kappa)} G_{\mu\nu}^{(\kappa)}(\mathbf{D}) + \sum_{\kappa=1}^3 D_{\mu\nu}^{\infty,(\kappa)} h_{\text{PV},\mu\nu}^{(\kappa)} \right] \right\}, \end{aligned} \quad (26)$$

where, ∞ refers to density matrices obtained variationally in the presence of the perturbation, which is analogous to an infinite order perturbation theory treatment of \hat{H}_{PV} (for details

see Eq. (A3) in the Appendix), provided that this converges. Thus, the gradient with respect to nuclear displacements can be written as

$$\begin{aligned}
\vec{\nabla}_{\vec{\eta}} E_{\infty} = \Re \left\{ \sum_{\mu\nu} \left[\sum_{\kappa=0}^3 \left(\vec{\nabla}_{\vec{\eta}} D_{\mu\nu}^{\infty,(\kappa)} \right) h_{ZORA,\mu\nu}^{(\kappa)} + \sum_{\kappa=0}^3 D_{\mu\nu}^{\infty,(\kappa)} \left(\vec{\nabla}_{\vec{\eta}} h_{ZORA,\mu\nu}^{(\kappa)} \right) \right. \right. \\
+ \frac{1}{2} \sum_{\kappa=0}^3 \left(\vec{\nabla}_{\vec{\eta}} D_{\mu\nu}^{\infty,(\kappa)} \right) G_{\mu\nu}^{(\kappa)}(\mathbf{D}^{\infty}) + \frac{1}{2} \sum_{\kappa=0}^3 D_{\mu\nu}^{\infty,(\kappa)} \left(\vec{\nabla}_{\vec{\eta}} G_{\mu\nu}^{(\kappa)}(\mathbf{D}^{\infty}) \right) \\
\left. \left. + \sum_{\kappa=1}^3 \left(\vec{\nabla}_{\vec{\eta}} D_{\mu\nu}^{\infty,(\kappa)} \right) h_{PV,\mu\nu}^{(\kappa)} + \sum_{\kappa=1}^3 D_{\mu\nu}^{\infty,(\kappa)} \left(\vec{\nabla}_{\vec{\eta}} h_{PV,\mu\nu}^{(\kappa)} \right) \right] \right\} \quad (27)
\end{aligned}$$

For a first order property that does not depend on the basis functions such as the parity-violating potential, this expres-

sion can be simplified by using the orthonormality condition of the HF equations and with Eq. (13) we receive the leading order parity-violating energy gradient (see Appendix C):

$$\vec{\nabla}_{\vec{\eta}} E_{PV} \approx \Re \left\{ \sum_{\mu\nu} \left[\sum_{\kappa=0}^3 D_{\mu\nu}^{(\kappa)} \left(\vec{\nabla}_{\vec{\eta}} h_{ZORA,\mu\nu}^{(\kappa)} \right) + \sum_{\kappa=0}^3 D_{\mu\nu}^{(\kappa)} \vec{G}_{\text{grad},\mu\nu}^{(\kappa)}(\mathbf{D}, \mathbf{D}') + \sum_{\kappa=1}^3 D_{\mu\nu}^{(\kappa)} \left(\vec{\nabla}_{\vec{\eta}} h_{PV,\mu\nu}^{(\kappa)} \right) - W_{\mu\nu}^{(0)} \left(\vec{\nabla}_{\vec{\eta}} S_{\mu\nu} \right) \right] \right\}. \quad (28)$$

where we have introduced the energy weighted density matrix (EWDM) \mathbf{W} as

$$\mathbf{W}^{(\kappa)} = \sum_{i=1}^{N_{\text{orb}}} n_i \varepsilon_i \mathbf{D}_i^{(\kappa)}, \quad (29)$$

and the matrix $\vec{\mathbf{G}}_{\text{grad}}^{(\kappa)}$ of contracted gradients of two-electron integrals with elements:

$$\vec{G}_{\text{grad},\mu\nu}^{(\kappa)}(\mathbf{D}, \mathbf{D}') = \sum_{\rho\sigma} \left[\delta_{k0} D_{\rho\sigma}^{(\kappa)} \vec{\nabla}_{\vec{\eta}} (\mu\nu | \rho\sigma) - a_X \frac{1}{2} D_{\rho\sigma}^{(\kappa)} \vec{\nabla}_{\vec{\eta}} (\mu\sigma | \rho\nu) + 2a_{\text{DFT}} \left\langle \chi_{\mu} \left| \hat{V}'_{\text{XC}}(\mathbf{D}, \mathbf{D}') \right| \vec{\nabla}_{\vec{\eta}} \chi_{\nu} \right\rangle \right]. \quad (30)$$

Note, that in the DFT case, derivatives of the exchange-correlation potential have to be computed for the calculation of the perturbed two-electron gradients, which in the spin-polarised LDA case are

$$V'_{\text{XC,LDA}}(\mathbf{D}^{(0)}, \mathbf{D}'^{(0)}) = \frac{\delta V_{\text{XC,LDA}}(\mathbf{D}^{(0)})}{\delta \rho(\vec{r}; \mathbf{D}^{(0)})} \rho(\vec{r}; \mathbf{D}'^{(0)}). \quad (31)$$

For other functionals see Appendix B. \mathbf{D} is the SCF density matrix of the unperturbed system, i.e. received with the Hamiltonian \hat{H}_0 only, and \mathbf{D}' and \mathbf{W}' are the perturbed density matrix and EWDM of first order in λ_{PV} .

The nuclear displacement gradients of the full unperturbed ZORA Hamiltonian, i.e. the gradients of one-electron ZORA integrals $\vec{\nabla}_{\vec{\eta}} h_{ZORA,\mu\nu}^{(\kappa)}$, as well as gradients of two-electron integrals and the exchange-correlation potentials needed for $\vec{G}_{\text{grad},\mu\nu}^{(\kappa)}(\mathbf{D})$ have been implemented in Ref. 65. In this work, we have altered the previous one-electron gradient part to account also for a finite nucleus model when computing the derivatives of the one-electron integrals. What remains then to be obtained are the perturbed density matrices $\mathbf{D}'^{(\kappa)}$, the perturbed spin-independent EWDM $\mathbf{W}'^{(0)}$ and the gradient of the PV integrals $\vec{\nabla}_{\vec{\eta}} h_{PV,\mu\nu}^{(\kappa)}$. We describe the scheme for computing the latter in the following subsection II A, before we discuss in subsection II B the linear response scheme that is

used for computation of perturbed density matrices.

A. Gradient of the PV integrals

The matrix elements of the one electron PV operator in basis set representation is

$$\begin{aligned}
h_{\text{PV},\mu\nu}^{(\kappa)} &= \left\langle \chi_{\mu,B} \left| \hat{h}_{\text{PV}}^{(\kappa)} \right| \chi_{\nu,C} \right\rangle \\
&= i\hbar \frac{G_{\text{F}}}{2\sqrt{2}} \sum_{A=1}^{N_{\text{nuc}}} \left\langle \chi_{\mu,B} \left| \hat{h}_{\text{PV},A}^{(\kappa)} \right| \chi_{\nu,C} \right\rangle \\
&= i\hbar \frac{G_{\text{F}}}{2\sqrt{2}} \sum_{A=1}^{N_{\text{nuc}}} \left(\left\langle \chi_{\mu,B} \left| \omega(\vec{r}) Q_{\text{W},A} \rho_{\text{nuc},A}(\vec{r}) \right| \partial_{\kappa} \chi_{\nu,C} \right\rangle \right. \\
&\quad \left. - \left\langle \partial_{\kappa} \chi_{\mu,B} \left| \omega(\vec{r}) Q_{\text{W},A} \rho_{\text{nuc},A}(\vec{r}) \right| \chi_{\nu,C} \right\rangle \right) \quad (32)
\end{aligned}$$

with $\partial_{\kappa} = \frac{\partial}{\partial x^{\kappa}}$ denoting a component of the electronic four derivative, with the four vector being $x^{(0,1,2,3)} = (ct, x, y, z)^{\text{T}}$. Indices A, B, C denote the nuclei at which the basis functions χ or nuclear density distribution ρ_{nuc} are hooked. As the basis functions depend on the nuclear coordinates, the geometry

gradient of the PV integrals is

$$\begin{aligned} \vec{\nabla}_{\vec{\eta}} h_{\text{PV},A,\mu\nu}^{(\kappa)} &= \left\langle \vec{\nabla}_{\vec{\eta}} \chi_{\mu,B} \left| \hat{h}_{\text{PV},A}^{(\kappa)} \right| \chi_{\nu,C} \right\rangle \\ &+ \left\langle \chi_{\mu,B} \left| \vec{\nabla}_{\vec{\eta}} \hat{h}_{\text{PV},A}^{(\kappa)} \right| \chi_{\nu,C} \right\rangle \\ &+ \left\langle \chi_{\mu,B} \left| \hat{h}_{\text{PV},A}^{(\kappa)} \right| \vec{\nabla}_{\vec{\eta}} \chi_{\nu,C} \right\rangle \end{aligned} \quad (33)$$

where, the second term is the Hellmann-Feynman term and the first and third term are the basis function contributions. The integrals of the PV operator are purely imaginary and due to Hermiticity of the PV operator, the basis function contributions are connected by

$$\left\langle \vec{\nabla}_{\vec{\eta}} \chi_{\mu,B} \left| \hat{h}_{\text{PV},A}^{(\kappa)} \right| \chi_{\nu,C} \right\rangle = - \left\langle \chi_{\nu,C} \left| \hat{h}_{\text{PV},A}^{(\kappa)} \right| \vec{\nabla}_{\vec{\eta}} \chi_{\mu,B} \right\rangle. \quad (34)$$

$$\left\langle \chi_{\mu,B} \left| \hat{h}_{\text{PV},A}^{(\kappa)} \right| \vec{\nabla}_D \chi_{\nu,C} \right\rangle = i\hbar \frac{G_F}{2\sqrt{2}} \delta_{DC} \sum_{A=1}^{N_{\text{nuc}}} \left(- \left\langle \chi_{\mu,B} \left| \omega(\vec{r}) Q_{W,A} \rho_{\text{nuc},A}(\vec{r}) \right| \vec{\nabla} \partial_{\kappa} \chi_{\nu,C} \right\rangle + \left\langle \partial_{\kappa} \chi_{\mu,B} \left| \omega(\vec{r}) Q_{W,A} \rho_A(\vec{r}) \right| \vec{\nabla} \chi_{\nu,C} \right\rangle \right). \quad (35)$$

For a Gaussian shaped nuclear density distribution, the Hellmann-Feynman term reads

$$\begin{aligned} \left\langle \chi_{\mu,B} \left| \vec{\nabla}_D \hat{h}_{\text{PV}}^{(\kappa)} \right| \chi_{\nu,C} \right\rangle &= i\hbar \frac{G_F}{2\sqrt{2}} \left(- \left\langle \chi_{\mu,B} \left| -(\vec{\nabla}_D \omega(\vec{r})) \sum_A Q_{W,A} \rho_A(\vec{r}) + \omega(\vec{r}) Q_{W,D} (\vec{\nabla} \rho_D(\vec{r})) \right| \partial_{\kappa} \chi_{\nu,C} \right\rangle \right. \\ &\left. + \left\langle \partial_{\kappa} \chi_{\mu,B} \left| -\vec{\nabla}_D \omega(\vec{r}) \sum_A Q_{W,A} \rho_A(\vec{r}) + \omega(\vec{r}) Q_{W,D} (\vec{\nabla} \rho_D(\vec{r})) \right| \chi_{\nu,C} \right\rangle \right), \end{aligned} \quad (36)$$

with the gradient of a Gaussian normalised nuclear density distribution being

$$\vec{\nabla} \rho_A(\vec{r}) = -2\zeta_A \left(\frac{\zeta_A}{\pi} \right)^{3/2} (\vec{r} - \vec{R}_A) \exp \left\{ -\zeta_A |\vec{r} - \vec{R}_A|^2 \right\}. \quad (37)$$

The geometry gradient of the ZORA factor $\vec{\nabla}_A \omega$ is discussed in Ref. 62. The construction of ZORA, PV operators and its derivatives is done by means of numerical integration.

The above integrals are evaluated numerically on a grid. In the present work, an atom centered grids is used employing the Treuter-Ahlrichs⁶⁶ version of a Becke grid,⁶⁷ where the partitioning is done by weight functions w_i for each grid point i . As these weight functions depend on the nuclear coordinates they give an additional contribution to the PV gradient which is calculated as

$$\sum_i^{N_{\text{grid}}} \left(\chi_{\mu,B}(\vec{r}_i) \hat{h}_{\text{PV},A}^{(\kappa)}(\vec{r}_i) \chi_{\nu,C}(\vec{r}_i) \right) \vec{\nabla}_{\vec{\eta}} w_i(\vec{R}) \quad (38)$$

The grid points move when the nuclei are slightly displaced. To account for this effect, we employ that translational invariance of the molecule holds and, therewith, the net force on the molecule has to be zero. We, therefore, subtract the

We split the nuclear displacements $\vec{\eta}$ into the separate contributions from different nuclei A . The basis functions depend on $\vec{r} - \vec{R}_A$. Therefore, only the subset of basis functions centered at A contributes to the corresponding integrals. Furthermore, as we deal with Gaussian basis functions, derivatives with respect to nuclear coordinates can be represented by derivatives with respect to electronic coordinates as $\partial_{A,\kappa} \chi_B = -\delta_{AB} \partial_{\kappa} \chi_B$, where $\partial_{A,\kappa}$ denotes a component of the four derivative of nucleus A . For the basis function contribution to the PV gradient integrals, we arrive at

net force that results from the numerical integration procedure from the numerically integrated gradient contribution $(\vec{\nabla}_D h_{\text{PV},A,\mu\nu}^{(\kappa)})_{\text{num}}$:

$$\vec{\nabla}_D h_{\text{PV},A,\mu\nu}^{(\kappa)} = (\vec{\nabla}_D h_{\text{PV},A,\mu\nu}^{(\kappa)})_{\text{num}} - \sum_B (\vec{\nabla}_B h_{\text{PV},A,\mu\nu}^{(\kappa)})_{\text{num}}. \quad (39)$$

B. Linear response computation of perturbed density matrices

In first order the perturbed density matrix can be written in terms of the unoccupied-occupied block \mathbf{T}_{uo} of an anti-Hermitian transformation matrix \mathbf{T} (see Appendix D 1 for details):

$$D_{\mu\nu}^{(\kappa)}(\mathbf{T}_{\text{uo}}) = \sum_i^{\text{occ}} \sum_a^{\text{unocc}} \left[\vec{C}_{\mu a}^{\dagger} \sigma^{(\kappa)} \vec{C}_{\nu i} T_{ai}^* + \vec{C}_{\nu i}^{\dagger} \sigma^{(\kappa)} \vec{C}_{\mu a} T_{ai} \right]. \quad (40)$$

For how to compute perturbed density matrices to arbitrary order see Ref. 68.

We introduce the MO transformed PV operator as

$$H_{\text{PV,MO},ij} = \sum_{\kappa=1}^3 \sum_{\mu\nu} \vec{C}_{\mu i}^\dagger \sigma^\kappa \vec{C}_{\nu j} h_{\text{PV},\mu\nu}^{(\kappa)}. \quad (41)$$

If we would assume that the first order perturbed wave function would be calculated by transformation of the orbital coefficients as

$$\vec{C}_{\mu i}^i \approx \sum_a^{\text{unocc}} \vec{C}_{\mu a} (\varepsilon_a - \varepsilon_i)^{-1} H_{\text{PV,MO},ai} \quad (42)$$

then the perturbed density matrix would simply be calculated as $D_{\mu\nu}^{(\kappa)} (\Delta^{-1} \circ \mathbf{H}_{\text{PV,MO}}^{\text{uo}})$ with \circ being the Hadamard product and the matrices Δ , Δ^{-1} having the elements $\Delta_{ai} = (\varepsilon_a - \varepsilon_i)$ and $\Delta_{ai}^{-1} = (\varepsilon_a - \varepsilon_i)^{-1}$, respectively. Here a and i are defined in the space of unoccupied and occupied orbitals, respectively.

However, this does not account for the response of the orbitals to the perturbation but correspond to a simple sum over states approach in which it is assumed that the electronic Hessian is diagonal and therefore the perturbed SCF equations are uncoupled. Within HF and KS, however, the electronic Hessian is not diagonal as the two-electron matrix \mathbf{G} is a function of the orbitals and one has to solve the coupled perturbed HF (CPHF) or coupled perturbed KS (CPKS) equations (see Appendix D 2 and for a detailed derivation e.g. Ref.69). To solve the response equations, we use the reduced form (see Refs. 70 and 71 and Appendix D 2 for details):

$$\sum_{bj} \mathbf{A}_{bj} T_{bj} + \mathbf{B}_{bj} T_{bj}^* = -\mathbf{H}_{\text{PV,MO}}^{\text{uo}} \quad (43)$$

where indices b run over unoccupied orbitals and indices j over occupied orbitals. The elements of the electronic Hessian are

$$A_{ai,bj} = (\varepsilon_a - \varepsilon_i) \delta_{ab} \delta_{ij} + \tilde{G}_{ai,jb} \quad (44)$$

$$B_{ai,bj} = \tilde{G}_{ai,bj}, \quad (45)$$

with $\tilde{G}_{ai,bj}$ being an element of the four-index MO transformed two-electron tensor:

$$\tilde{G}_{ai,bj} = \sum_{\kappa=0}^3 \sum_{\mu\nu} D_{ai\mu\nu}^{(\kappa)} G_{\mu\nu}^{(\kappa)} (\mathbf{D}_{bj}), \quad (46)$$

with the transition density matrix \mathbf{D}_{ai} having the elements

$$D_{ai,\mu\nu}^{(\kappa)} = \vec{C}_{\mu a}^\dagger \sigma^\kappa \vec{C}_{\nu i}. \quad (47)$$

Eq. (43) is solved iteratively within a preconditioned conjugate gradient algorithm. Thereby, as initial guess (0), we employ trial vectors $\tilde{\mathbf{T}}$ that represent the uncoupled solutions:

$$\tilde{\mathbf{T}}^{(0)} = -\mathbf{H}_{\text{PV,MO}}^{\text{uo}} \circ \Delta^{-1} \quad (48)$$

$$\mathbf{R}^{(0)} = \tilde{\mathbf{T}}^{(0)} \circ \Delta \quad (49)$$

$$\mathbf{P}^{(0)} = \tilde{\mathbf{T}}^{(0)}. \quad (50)$$

In an iterative procedure in each step i from the trial vector $\tilde{\mathbf{T}}^{(i-1)}$, we construct the perturbed density matrices $(\mathbf{D}^{(\kappa)})^{(i)}$

following Eq. (40) and calculate the contracted electronic Hessian as

$$\tilde{\mathbf{E}}^{[2],(i)} = \tilde{\mathbf{T}}^{(i-1)} \circ \Delta + \mathbf{G}_{\text{MO}}^{\text{uo}} (\mathbf{D}'(\tilde{\mathbf{T}}^{(i-1)})), \quad (51)$$

with the two-index MO transformed two-electron matrix:

$$G_{\text{MO},ai}(\mathbf{D}') = \sum_{\kappa=0}^3 \sum_{\mu\nu} \vec{C}_{\mu a}^\dagger \sigma^\kappa \vec{C}_{\nu i} G_{\mu\nu}^{(\kappa)}(\mathbf{D}'), \quad (52)$$

From this we update

$$\alpha^{(i)} = \frac{r^{(i-1)}}{\text{Tr} \left((\tilde{\mathbf{T}}^{(i-1)})^\dagger \tilde{\mathbf{E}}^{[2],(i)} \right)} \quad (53)$$

$$\mathbf{R}^{(i)} = \mathbf{R}^{(i-1)} - \alpha^{(i)} \tilde{\mathbf{E}}^{[2],(i)} \quad (54)$$

$$\mathbf{P}^{(i)} = -\mathbf{R}^{(i)} \circ \Delta^{-1} \quad (55)$$

$$r^{(i)} = \left| \text{Tr} \left((\mathbf{R}^{(i)})^\dagger \mathbf{P}^{(i)} \right) \right| \quad (56)$$

For all calculations in this paper, the Fletcher-Reeves weight of the precondition was employed, which is calculated as $\beta_{\text{FR}} = \frac{r^{(i)}}{r^{(i-1)}}$ and the algorithm is followed until convergence of the norm $\sqrt{\frac{r^{(i)}}{r^{(0)}}}$ to a given threshold.

The trial matrix is updated as

$$\tilde{\mathbf{T}}^{(i)} = \mathbf{P}^{(i)} + \beta \tilde{\mathbf{T}}^{(i-1)}. \quad (57)$$

Upon convergence, the solution is received as the sum over all weighted trial matrices from the N_{iter} iterations:

$$\mathbf{T}_{\text{uo}} = \sum_{i=1}^{N_{\text{iter}}} \alpha^{(i)} \tilde{\mathbf{T}}^{(i-1)} \quad (58)$$

From the solution vectors of the linear response equations \mathbf{T} , new perturbed density matrices are calculated following Eq. (40) and the perturbed EWDM can be calculated as

$$W_{\mu\nu}^{\prime(\kappa)}(\mathbf{T}_{\text{uo}}) = \sum_i^{\text{occ}} \sum_a^{\text{unocc}} \left[\vec{C}_{\mu a}^\dagger \sigma^{(\kappa)} \vec{C}_{\nu i} (\varepsilon_i T_{ai}^* + (F'_{ai})^*) + \vec{C}_{\nu i}^\dagger \sigma^{(\kappa)} \vec{C}_{\mu a} (\varepsilon_i T_{ai} + F'_{ai}) \right], \quad (59)$$

with the MO transformed Fock matrix being

$$\mathbf{F}' = \mathbf{H}_{\text{PV,MO}}^{\text{uo}} + \mathbf{G}_{\text{MO}}^{\text{uo}}(\mathbf{D}'(\mathbf{T}_{\text{uo}})). \quad (60)$$

In case of DFT contributions from the exchange correlation potential to the perturbed \mathbf{G} matrix have to be calculated via derivatives of the exchange correlation potential as shown as in 31 for the case of spin unpolarised LDA; for a more general discussion of exchange-correlation functionals see Appendix B and Ref. 70).

III. COMPUTATIONAL DETAILS

In the pilot implementation of the PV energy gradient, unperturbed LCAO coefficients (\mathbf{C}), orbital energies (ε), PV operators as well as two electron integrals (\mathbf{G}) were computed

with a modified version^{62,64,72,73} of the Turbomole program package.^{74,75} Therein, the conjugate gradient algorithm for solving the linear response equations [Eqs. (48-58)] was implemented within MATLAB⁷⁶ and the modified Turbomole program was called to compute the perturbed \mathbf{G} matrix in AO basis following Eq. (22). The resulting perturbed density matrices [Eqs. (40) and (59)] were used in a modified version of the gradient implementation of Ref. 65 to assemble the analytic gradient of the parity-violating potential.

The calculation of the two-electron part (HF case and Coulomb contribution in LDA) of the perturbed contracted two-electron matrix \mathbf{G} is carried out via contraction of the two electron tensor $(\mu\nu|\rho\sigma)$ with the two-particle density matrix $\Gamma^{(\kappa,\lambda)}$ which can be constructed from the one-particle density matrices as

$$\Gamma_{\mu\nu\rho\sigma}^{(\kappa,\lambda)}(\mathbf{D}^{(\kappa)}, \mathbf{D}^{(\lambda)}) = a_C^{\kappa,\lambda} D_{\mu\nu}^{(\kappa)} D_{\rho\sigma}^{(\lambda)} - a_X^{\kappa,\lambda} \frac{1}{2} D_{\mu\sigma}^{(\kappa)} D_{\rho\nu}^{(\lambda)} \quad (61)$$

Note, that for the employed ZORA operator without two-

electron spin-orbit or spin-spin coupling terms, only two-electron densities with $\kappa = \lambda$ are required at the HF or DFT level. Furthermore, we introduced the scaling factors for the direct Coulomb contribution $a_C^{\kappa,\lambda}$, which is in all present calculations set as $a_C^{\kappa,\lambda} = \delta_{0\kappa}\delta_{0\lambda}$ and a more flexible scaling parameter for the exchange contribution $a_X^{\kappa,\lambda}$, which is in the present implementation set to be constant $a_X^{\kappa,\lambda} = a_X$.

For the calculation of the two-electron contribution to the PV energy gradient, the perturbed two particle density matrices are needed:

$$\Gamma_{\mu\nu\rho\sigma}^{(\kappa,\lambda)} = \Gamma_{\mu\nu\rho\sigma}^{(\kappa,\lambda)}(\mathbf{D}'^{(\kappa)}, \mathbf{D}^{(\lambda)}) = a_C^{\kappa,\lambda} D_{\mu\nu}'^{(\kappa)} D_{\rho\sigma}^{(\lambda)} - a_X^{\kappa,\lambda} \frac{1}{2} D_{\mu\sigma}'^{(\kappa)} D_{\rho\nu}^{(\lambda)} \quad (62)$$

Whereas in the present implementation Eq. (62) is employed directly, in the pilot implementation the perturbed two-electron density matrices were calculated for practical reasons via

$$\Gamma_{\mu\nu\rho\sigma}'^{(\kappa,\lambda)} \simeq \frac{1}{2} \left[\Gamma_{\mu\nu\rho\sigma}^{(\kappa,\lambda)}(\mathbf{D}^{(\kappa)} + \mathbf{D}'^{(\kappa)}, \mathbf{D}^{(\lambda)} + \mathbf{D}'^{(\lambda)}) - \Gamma_{\mu\nu\rho\sigma}^{(\kappa,\lambda)}(\mathbf{D}^{(\kappa)}, \mathbf{D}^{(\lambda)}) - \Gamma_{\mu\nu\rho\sigma}^{(\kappa,\lambda)}(\mathbf{D}'^{(\kappa)}, \mathbf{D}'^{(\lambda)}) \right], \quad (63)$$

where a constant, numerical scaling factor of $2\sqrt{2}/[\alpha G_F/(E_h a_0^3)] \approx 1.74 \times 10^{16}$ was used to scale up artificially the very small numerical values in the perturbed density matrices to avoid subtractive cancellation in Eq. 63.

The present implementation of $\vec{\nabla}E_{PV}$ as defined in Eq. (28) as well as the response equations [Eqs. (48-58)] were included in a modified version^{63,77} of the Turbomole program.^{74,75} The results from the current production-level implementation are identical to those of the pilot implementation. The two different implementations provided an internal test of our results. The implementation proceeds as follows:

1. For a given molecular structure, unperturbed LCAO coefficients and orbital energies are received from a SCF computation at the two-component ZORA level with the modified version^{62,64,72,73} of Turbomole^{74,75} and written on disk.
2. Integrals of the PV operator [Eq. (32)] are computed and from this the initial guess for the response equations is formed [Eq. (41)] with the program described in Ref. 77.
3. The linear response equations are solved in an iterative manner following Eqs. (48-58) within the program of Ref. 77 and the perturbed density matrices and perturbed energy weighted density matrix are written on disk.
4. Within a modified version of the program described in Ref. 65 the gradient integrals of the PV operator [Eq. (33-38)], of the ZORA operator $\vec{\nabla}_{\vec{\eta}} h_{ZORA,\mu\nu}^{(\kappa)}$ and of the

two-electron integrals $\vec{\nabla}_{\vec{\eta}}(\mu\nu|\rho\sigma)$ are computed and combined with the unperturbed and perturbed density matrices following Eq. (28). For two-electron contributions the perturbed two electron matrix is formed [Eq. (62)] and contracted with the gradient of two-electron integrals $\vec{\nabla}_{\vec{\eta}}(\mu\nu|\rho\sigma)$.

In the following, the scheme described above for computing $\vec{\nabla}E_{PV}$ is used to study electroweak parity-violating effects in halogenated methane derivatives; CHBrCIF, CHClFI, CHBrFI and CHAtFI. As mentioned in the Introduction, their vibrational spectra, in particular for CHBrCIF have been extensively studied theoretically^{34-36,38,40,51,52} and experimentally^{14,16,17,42,49} to detect PV effects. A high resolution of 5×10^{-14} has been achieved for the C-F stretching mode of CHBrCIF with CO₂ laser spectroscopy,⁴² which is nevertheless about three or four orders of magnitude larger than the theoretical predictions of the size of the effect for the molecule under investigation. Therefore, the vibrational and rotational spectra of heavier homologues will be studied herein, as has been done previously for the vibrational frequency shifts in a one-dimensional anharmonic approximation.⁴⁰ Whereas in the previous work single-mode anharmonic effects were included variationally by solving the one-dimensional anharmonic vibrational Schrödinger equation, we will use in the present work vibrational perturbation theory to account for anharmonic effects. Most importantly, we can include now also multi-mode contributions to parity-violating frequency shifts efficiently, which were neglected in essentially all previous studies on parity-violating frequency shifts in chiral molecules with the notable exceptions of Ref. 53, where CDBrCIF was studied in a four-

dimensional anharmonic model that span the C–F stretching as well as C–D stretching and the two C–D bending modes and of Ref. 78, where up to third order vibrational effects in chiral arsenic and lead compounds were studied.

For all the methane derivatives mentioned above, we use the same molecular structures, electronic structure methods and basis sets from earlier work⁴⁰ to allow for direct comparison. As in Ref. 40, the *S*-enantiomers of a given chiral compound is considered when parity-violating potentials, and in the current work also gradients of the parity-violating potentials, are reported. Splittings of a property A between enantiomers are given as $\Delta A = A^S - A^R$. The equilibrium structures, harmonic vibrational frequencies and potential energy surfaces (PES) were computed on the CCSD(T) level with the cc-pVDZ basis set for the first to third row elements and quasi-relativistic Stuttgart pseudopotentials in the neutral atom reference system together with energy optimised valence basis sets for Br, I⁷⁹ and At.⁸⁰ Equilibrium structures, harmonic vibrational frequencies, corresponding normal coordinates and displaced structures as reported in Ref. 40 were reused in the present work. The PES have been determined by the SURF module⁵⁴ of MOLPRO.^{81–83} The double zeta basis is expected to behave comparatively poorly, but is kept herein to speed up the calculations and to obtain results that are directly comparable to previous work. An improved description of the anharmonic PES, in particular for the promising astatine containing methane derivative will be left for a later study.

In computations of the PV operator a Weinberg parameter of $\sin^2 \theta_W = 0.2319$ has been used to determine the weak nuclear charge $Q_{W,A} = (1 - 4\sin^2 \theta_W)Z_A - N_A$, with Z_A being the number of protons and N_A being the number of neutrons in nucleus A . In all two-component ZORA calculations an even tempered basis set, with the exception of an uncontracted aug-cc-pVDZ basis set for hydrogen, has been used in order to compare the results to previous works.^{40,84} The parameters of the even tempered series are $\alpha_i = \gamma\beta_N^{N-i}$, $i = 1, \dots, N$, with $N = 26$, $\gamma = 0.02$ and $\alpha_1 = 500000000$. For s and p functions, the exponents α_{1-25} and α_{2-26} have been used, while in the case of d functions, α_{20-24} has been chosen for elements of the second and third row of the periodic table of elements, α_{15-25} for the fourth and fifth row and α_{12-25} for the sixth row, which is the only one to contain f functions as well with exponents α_{15-22} .

For LDA, Dirac exchange⁸⁵ and VWN5 correlation⁸⁶ potentials have been used. For LDA a standard DFT integration grid was used, whereas matrix elements of the ZORA and PV operators were computed on a very dense grid. MOs have been converged until the change of the SCF energy and relative change of spin-orbit energy (except CHCIF1 at HF level) between two-successive iterations dropped below at least $10^{-6} E_h$ and 10^{-12} respectively. MOs for CHCIF1 at HF level have been converged to less than 10^{-15} for the relative spin-orbit energy change as the corresponding PV energy for the equilibrium structure was not converged to the desired accuracy with the 10^{-12} criterion. In practice, the spin-orbit energy criterion was by far the more restrictive one, such that at the end of the iterative process, the change in SCF energy between two cycles typically dropped below $10^{-9} E_h$. The

threshold for negelection of gradients of two-electron integrals was set to $10^{-15} E_h a_0^{-1}$.

Following the regular spectroscopic notation, the normal modes of the methane derivatives are named in descending order of the frequency values.

IV. RESULTS AND DISCUSSION

We first make a comparison of the directional derivatives of the PV energy along the C–F stretching mode (v_4) as obtained from the analytical PV energy gradients with those of the numerical ones from an earlier study.⁴⁰ The PV energy gradients are utilised for estimating the shifts of the rotational constants corresponding to the equilibrium structures. The vibrational frequency shifts in vibrational transitions for the C–F stretching mode are calculated within a perturbative treatment using the PV energy gradients. At the end, the multi-mode effects in the vibrational transitions for all the normal modes in CHBr-CIF and CHAtFI molecules are discussed.

A. PV energy gradients

All the chiral methane derivatives studied here show a characteristic C–F stretching mode (v_4) which is amenable to high-resolution CO₂ laser spectroscopy. The directional derivative of the PV energy along the C–F stretching normal coordinate (q_4) is obtained herein by projecting the analytical Cartesian PV gradient $\vec{\nabla}E_{PV}$ onto the Cartesian displacement vector \hat{u}_{q_4} corresponding to a unit shift along the dimensionless reduced normal coordinate q_4 . Table I depicts the HF and LDA level directional derivative along C–F stretching mode at the equilibrium structure. See the Supporting Information for the corresponding Cartesian HF and LDA level $\vec{\nabla}E_{PV}$ for each of the equilibrium structures.

In general, the analytically computed gradient is expected to be more accurate than a numerical counterpart obtained by a finite difference scheme, provided that the underlying self-consistent field solutions are well converged. We note in reference to Table I, that a direct comparison of the analytical and numerical directional derivative of the parity violating potential is partially hampered by the fact that the analytical gradient is calculated at the equilibrium structure of the molecule, whereas the numerical directional derivative was determined in Ref. 40 from the linear term of a polynomial fit of the parity-violating potential as calculated along a one-dimensional cut along the C–F stretching normal coordinate q_4 in the range from -3 to 3 . The two become better comparable, if one computes also the analytical directional derivatives at several points along the same normal mode displacement and performs a polynomial fit. Therefore, as a next step, the coordinate dependence of the PV gradient is examined, checking the higher order terms as well, by fitting the $\vec{\nabla}E_{PV} \cdot \hat{u}_{q_r}$ to the third order polynomial.

$$\vec{\nabla}E_{PV}(q_r) \cdot \hat{u}_{q_r} \approx \sum_{i=0}^3 a_i q_r^i \quad (64)$$

TABLE I. Analytical directional derivative ($\vec{\nabla}E_{\text{PV}}(\vec{R}_0) \cdot \hat{u}_{q_4}$ in 10^{-12} cm^{-1}) along the dimensionless reduced normal coordinates corresponding to the C-F stretching mode (v_4) of the chiral halogenated methane derivatives as computed at the equilibrium structure.

molecules	$\vec{\nabla}E_{\text{PV}}(\vec{R}_0) \cdot \hat{u}_{q_4}$	HF	LDA
CHBrCIF	analytical	0.4205	0.4330
	numerical ^a	0.42148(5)	0.4333(2)
CHClFI	analytical	4.1407	2.9285
	numerical ^a	4.1452(9)	2.92880(4)
CHBrFI	analytical	7.0813	7.6584
	numerical ^a	7.0842(5)	7.65824(5)
CHAtFI	analytical	60.1744	-28.0288
	numerical ^a	59.91(5)	-27.63(7)

^a Numerical derivatives obtained in Ref. 40 from a polynomial fit of a one-dimensional cut through the parity-violating potential along the dimensionless reduced normal coordinates q_4 . For the equilibrium structure of CHClFI, however, the HF value was slightly less tightly converged, so that this value was recomputed herein (see supplement) and the potential refitted, leading to only slightly improved fit values.

where \hat{u}_{q_r} is the Cartesian displacement vector corresponding to a unit displacement along the normal coordinate q_r and a_i would correspond to $\frac{1}{i!} \left. \frac{\partial^i \vec{\nabla}E_{\text{PV}} \cdot \hat{u}_{q_r}}{\partial q_r^i} \right|_{q_r=0}$ in a Taylor series expansion of $\vec{\nabla}E_{\text{PV}} \cdot \hat{u}_{q_r}$. Thus, a_0 is similar to the value of the $\vec{\nabla}E_{\text{PV}} \cdot \hat{u}_{q_r}$ at the equilibrium structure along the normal mode v_r . The other fitting coefficients a_1 , a_2 and a_3 are related to the first, second and third order derivatives, respectively, of $\vec{\nabla}E_{\text{PV}} \cdot \hat{u}_{q_r}$ with respect to the dimensionless reduced normal coordinate q_r for v_r mode.

For this purpose, structures that are displaced along the normal coordinates of a vibrational mode are employed to generate a one-dimensional cut through the PV potential energy surface along q that varies from -3 to 3 through the equilibrium structure ($q = 0$). A total of 17 points is taken into consideration. Here, for each of the methane derivatives, we consider the one-dimensional cut for the C-F stretching mode (v_4). Figures 1–4 display the HF and LDA level $\vec{\nabla}E_{\text{PV}}(q_4) \cdot \hat{u}_{q_4}$ along the dimensionless reduced normal coordinates corresponding to the C-F stretching mode of the methane derivatives. The corresponding numerical values of $\vec{\nabla}E_{\text{PV}}(q_4) \cdot \hat{u}_{q_4}$ are given in Tables S15-S18 in the Supporting Information file. The fitting coefficients need to be adapted to compare the structure dependence of the PV energy $E_{\text{PV}}(\vec{q}_r)$ with the directional derivative of the PV energy $\vec{\nabla}E_{\text{PV}} \cdot \hat{u}_{q_4}$ along the dimensionless reduced normal coordinates q_4 corresponding to the C-F stretching mode, because the former can be fitted to a polynomial expansion, too, namely

$$E_{\text{PV}}(q_r) \approx \sum_{i=0}^4 b_i q_r^i, \quad (65)$$

TABLE II. Fitting coefficients of the HF PV energy (E_{PV}) and the HF PV energy gradients ($\vec{\nabla}E_{\text{PV}}$) along the C-F stretching mode (v_4) of the chiral halogenated methane derivatives in 10^{-12} cm^{-1} .

molecules	E_{PV}^a	$\vec{\nabla}E_{\text{PV}}$	
CHBrCIF	b_0	-1.4536(1)	
	b_1	0.42148(5)	0.4210(2) a_0
	b_2	-0.04242(9)	-0.0424(1) $a_1/2$
	b_4	0.00019(1)	0.00019(1) $a_3/4$
CHClFI	b_0	-13.7228(9)	
	b_1	4.1452(9)	4.145(2) a_0
	b_2	-0.3157(7)	-0.316(1) $a_1/2$
	b_3	0.0022(1)	0.0017(2) $a_2/3$
CHBrFI	b_4	0.00104(8)	0.0011(1) $a_3/4$
	b_0	-38.4858(5)	
	b_1	7.0842(5)	7.084(2) a_0
	b_2	-0.4819(4)	-0.4818(9) $a_1/2$
CHAtFI	b_3	0.00874(8)	0.0085(1) $a_2/3$
	b_4	0.00060(5)	0.00060(7) $a_3/4$
	b_0	-2314.06(5)	
	b_1	59.91(5)	59.9(2) a_0
CHAtFI	b_2	-69.48(4)	-69.46(9) $a_1/2$
	b_3	7.946(8)	7.97(1) $a_2/3$
	b_4	-0.350(4)	-0.353(6) $a_3/4$

^a Ref. 40; for CHClFI data see also footnote to Tab. I.

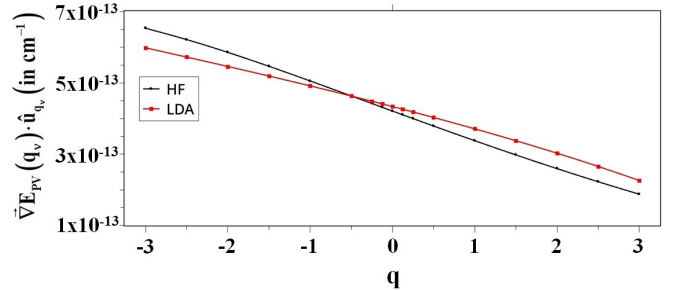


FIG. 1. HF and LDA level PV energy gradient (fitted to $\sum_{i=0}^3 a_i q_r^i$) along the C-F stretching mode of CHBrCIF. See Table II for the fitting coefficients (a_i) due to HF PV energy gradient. For the fitting coefficients of LDA PV energy gradient, see Table S23 in the Supporting Information.

where b_i would correspond to $\frac{1}{i!} \left. \frac{\partial^i E_{\text{PV}}(q_r)}{\partial q_r^i} \right|_{q_r=0}$ in a Taylor series expansion of E_{PV} . Thus, one has to contrast $E_{\text{PV}}(\vec{q}_r)$ with $\int \vec{\nabla}E_{\text{PV}}(q_r) \cdot \hat{u}_{q_r} dq_r$ and hence the values of a_0 , $a_1/2$, $a_2/3$ and $a_3/4$ are similar to the values of b_1 , b_2 , b_3 and b_4 respectively. The term b_0 corresponds in this approximation to the PV energy at the equilibrium structure.

The comparison of these fitting coefficients for PV energy (taken from Ref. 40) and directional derivative of the PV energy along the C-F stretching mode for the HF level is presented in Table II. Both numerical and analytical $\vec{\nabla}E_{\text{PV}} \cdot \hat{u}_{q_4}$ values for all the systems are in good agreement, with the numbers in parentheses denoting the error due to the fit pro-

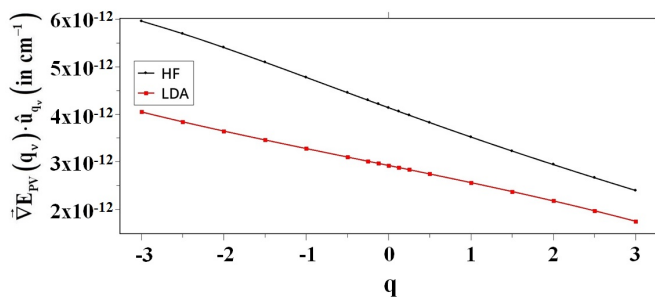


FIG. 2. HF and LDA level PV energy gradient (fitted to $\sum_{i=0}^3 a_i q_i^i$) along the C-F stretching mode of CHClFI. See Table II for the fitting coefficients (a_i) due to HF PV energy gradient. For the fitting coefficients of LDA PV energy gradient, see Table S23 in the Supporting Information.

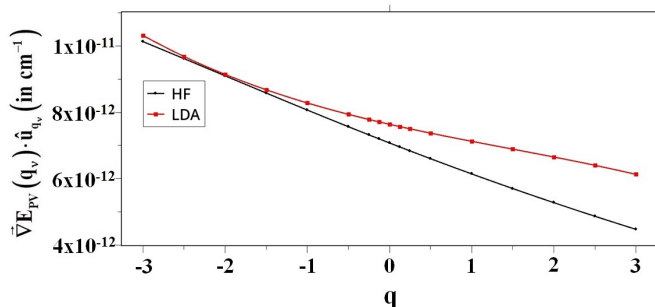


FIG. 3. HF and LDA level PV energy gradient (fitted to $\sum_{i=0}^3 a_i q_i^i$) along the C-F stretching mode of CHBrFI. See Table II for the fitting coefficients (a_i) due to HF PV energy gradient. For the fitting coefficients of LDA PV energy gradient, see Table S23 in the Supporting Information.

cedure, which involved one free parameter less for the directional derivative (eq. 64) than the PV potential (eq. 65). The corresponding comparisons of these fitting PV energy and PV energy gradient coefficients along the C-F stretching mode at the LDA level are given in the Supporting Information.

For the determination of the second partial derivatives

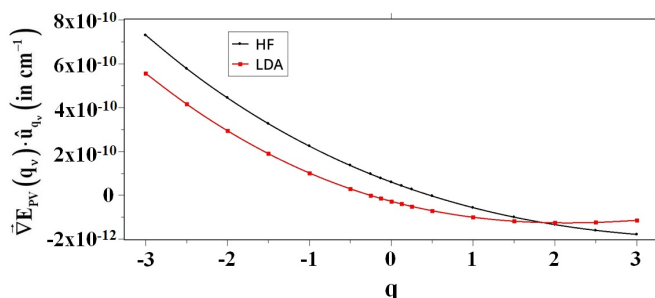


FIG. 4. HF and LDA level PV energy gradient (fitted to $\sum_{i=0}^3 a_i q_i^i$) along the C-F stretching mode of CHAtFI. See Table II for the fitting coefficients (a_i) due to HF PV energy gradient. For the fitting coefficients of LDA PV energy gradient, see Table S23 in the Supporting Information.

$\frac{\partial^2 E_{PV}}{\partial q_r^2}$ (same as a_1 in Table II), which are needed for calculating the vibrational energy levels as shown in Eqs. 8 and 9, one can expect the availability of the analytical gradient to simplify the calculations, because fewer points are needed from the PV energy surface. As a consistency check, a linear fit of the analytically calculated directional derivatives computed at $q = -0.125$, $q = 0$ and $q = 0.125$ has been opted for in all of the molecules, where the fitting values (a_1) are found to be in good agreement with the values presented in Table II. These linear fit values for the C-F stretching mode are reported [Table S22] in the Supporting Information.

B. Shifts of the rotational constants

The values shown in Tables I and II reveal that the equilibrium structure of these halogenated methane derivatives possess non-zero $\vec{\nabla}E_{PV}$. Due to these non-zero $\vec{\nabla}E_{PV}$ values, the PV potential can induce a minute change in the equilibrium structure. This leads to a shift of the rotational constants, which could in principle be measured by microwave spectroscopy. As already been discussed in the Introduction, the change of the structure and hence the shifts in the rotational constants due to the existence of non-zero $\vec{\nabla}E_{PV}$ at the minimum of the parity conserving potential is calculated with the help of the vibrational Hessian \mathbf{F} (see Eqs. 4 and 6). The change of the inertia tensor (ΔI_x) in the principal axis system and subsequently the change of the rotational constants (ΔX_R) can be approximated assuming that the result depends linearly on the displacements.³⁷

Shifts in the rotational constants as reported in Table III are highly sensitive to the PV energy gradients $\vec{\nabla}E_{PV}$. The numbers obtained on the LDA levels are found to be about one quarter of the HF results for the CHBrCIF molecule. The calculated relative effect in the microwave spectrum ($\Delta X/X \approx 10^{-17}$) of CHBrCIF, although it agrees well with the earlier finding by Quack and Stohner³⁴, is still far from the current experimental resolution. Similarly, the corresponding relative shifts in CHClFI and CHBrFI are about one order of magnitude larger in absolute value than for CHBrCIF, but still far below the present experimental resolution (see Table III). Considering the current scenario, the PV induced shifts of the rotational constants in CHBrCIF, CHClFI and CHBrFI are not expected to be measurable with present experimental setups. On the other hand, due to the heavy mass of astatine, a larger shift in the rotational constants is expected for CHAtFI. For this heavier At analogue, shifts are found to be about two or three-orders of magnitude higher in absolute value than the lighter molecules considered herein.

Another comment as to the accuracy of these estimates of rotational energy shifts is in order: Herein, we have followed the most simple approach³⁷ and computed only the PV shift at the equilibrium structure as it would arise from the PV gradient contribution. An improved treatment would include estimates of PV induced shifts of vibrationally averaged rotational constants as well as their influence on Coriolis coupling terms and centrifugal distortion constants.

TABLE III. Relative shift of the rotational constants in chiral halogenated methane derivatives.

	HF			LDA		
	$\Delta A/A$	$\Delta B/B$	$\Delta C/C$	$\Delta A/A$	$\Delta B/B$	$\Delta C/C$
CHBrCIF	2.093×10^{-17}	1.663×10^{-17}	2.111×10^{-17}	7.361×10^{-18}	4.291×10^{-18}	5.833×10^{-18}
CHClFI	1.438×10^{-16}	2.004×10^{-16}	2.171×10^{-16}	7.868×10^{-17}	8.091×10^{-18}	2.162×10^{-17}
CHBrFI	1.604×10^{-15}	1.818×10^{-16}	4.388×10^{-16}	1.472×10^{-15}	-1.374×10^{-16}	1.033×10^{-16}
CHAtFI	6.882×10^{-14}	1.300×10^{-15}	9.137×10^{-15}	1.271×10^{-14}	1.383×10^{-14}	1.395×10^{-14}

TABLE IV. Vibrationally averaged HF and LDA parity-violating potential $E_{n_4, \text{PV}}^S$ for energy levels n_4 in 10^{-12} cm^{-1} for the C-F stretching mode (ν_4) of the (S)-enantiomer of CHBrCIF, CHClFI, CHBrFI and CHAtFI.

Molecule	n_4	HF				LDA			
		Full 1D ^a	Perturbed 1D	Perturbed 2D	2D effects (%) ^b	Full 1D ^a	Perturbed 1D	Perturbed 2D	2D effects (%) ^b
CHBrCIF	0	-1.4328	-1.4326	-1.4211	-0.80	0.5621	0.5624	0.5802	3.17
	1	-1.3929	-1.3906	-1.3562	-2.47	0.6160	0.6192	0.6727	8.64
	2	-1.3554	-1.3485	-1.2912	-4.25	0.6668	0.6761	0.7652	13.18
	3	-1.3202	-1.3065	-1.2263	-6.14	0.7144	0.7329	0.8577	17.03
	1 \leftarrow 0	0.0399	0.0420	0.0649	54.53	0.0539	0.0568	0.0925	62.75
CHClFI	0	-13.463	-13.461	-13.445	-0.12	5.5610	5.5645	5.6159	0.92
	1	-12.953	-12.938	-12.890	-0.37	5.9640	5.9800	6.1342	2.58
	2	-12.459	-12.415	-12.336	-0.64	6.3500	6.3955	6.6525	4.02
	3	-11.979	-11.892	-11.781	-0.93	6.7170	6.8110	7.1708	5.28
	1 \leftarrow 0	0.510	0.523	0.555	6.07	0.4030	0.4155	0.5183	24.74
CHBrFI	0	-37.997	-37.996	-38.117	0.32	20.008	20.007	19.883	-0.62
	1	-37.035	-37.017	-37.380	0.98	21.311	21.306	20.932	-1.75
	2	-36.092	-36.037	-36.643	1.68	22.611	22.604	21.982	-2.75
	3	-35.169	-35.058	-35.906	2.42	23.904	23.903	23.032	-3.65
	1 \leftarrow 0	0.962	0.979	0.737	-24.74	1.303	1.299	1.050	-19.17
CHAtFI	0	-2343.3	-2343.4	-2320.3	-0.99	938.77	937.98	966.88	3.08
	1	-2401.2	-2402.2	-2332.9	-2.88	887.70	883.10	969.80	9.82
	2	-2458.1	-2461.0	-2345.5	-4.69	840.46	828.22	972.72	17.45
	3	-2513.8	-2519.7	-2358.0	-6.42	797.14	773.34	975.64	26.16
	1 \leftarrow 0	-57.9	-58.8	-12.6	-78.62	-51.07	-54.88	2.92	-105.3

^a Reference⁴⁰^b 2D effects = (Perturbed 2D - Perturbed 1D)/Perturbed 1D

C. Vibrational transitions for C-F stretching mode

For the vibrational spectrum, the results from the separable anharmonic adiabatic approximation (SAAA)³⁷ used in earlier work⁴⁰ have been compared to the one-dimensional (1D) perturbative approach (Eq. 9) of the present work. The influence of multi-mode coupling terms to the vibrational energy levels is also accounted for after adding the perturbative multi-mode contribution (Eq. 10) to the single-mode results. Table IV presents the vibrationally averaged HF and LDA parity violating potential energy levels up to 3rd vibrational state for the C-F stretching mode (ν_4) of the S-enantiomer of CHBrCIF, CHClFI, CHBrFI and CHAtFI molecules along with a comparison to SAAA results.⁴⁰

For the lowest transition (from $n_4 = 0$ to $n_4 = 1$) in CHBr-

CIF, the full 1D and the perturbative 1D treatment match to about $< 1 \%$, which is far below the accuracy of the employed ZORA-cGKS and ZORA-cGHF methods and therefore negligible. The transition after perturbative inclusion of multi-mode effects up to 2D coupling terms, however, differs by about 50 % (*cf.* Table IV). A similar influence of non-separable anharmonic effects on PV has been reported for similar molecules.⁵³ Nonetheless, the conclusion to be drawn is that the effect of the 2D treatment of the parity conserving potential is more important than the higher order terms of the 1D parity-violating potential. When comparing the different electronic structure methods, one finds significant differences, but the values for vibrational frequency shifts in CHBrCIF are in the same order of magnitude, deviating less than 30%, with the same sign, the latter of which is not the case

for the PV energy shifts. When compared with absolute values, the 2D contributions are found to increase for the higher vibrational levels. When these calculated PV frequency shifts (Table IV) are multiplied by two and then divided by the corresponding vibrational transition frequencies, they produce the dimensionless parity-violating relative vibrational frequency splittings between the C-F stretching fundamental of S- and R-enantiomers. The calculated relative vibrational frequency splittings corresponding to the lowest transition for the C-F stretching vibration of CHBrCIF molecule is found to be in good agreement with the earlier theoretical values.^{34–36,38,40,52}

For CHClFI, these parity-violating $1 \leftarrow 0$ transition frequency shifts are found to be about one order of magnitude higher than CHBrCIF (See Table IV). Again, the shifts in vibrational energy levels from the full and perturbed 1D treatment match better with each other, whereas the values obtained after inclusion of 2D contributions differ by a larger margin as compared to perturbative 1D treatment. Substitution with the heavier element bromine to CHBrCIF in place of chlorine leads to an increase of the PV transition frequency shifts compared to CHClFI again, which is not quite an order of magnitude this time (*cf.* Table IV). PV transition frequency shifts in the C-F stretching fundamental of CHBrFI due to full 1D and perturbed 1D are roughly twice to that of the values for CHClFI, whereas perturbed 2D effects in CHBrFI measures about 75% higher than the 2D contributions in CHClFI molecule. Akin to CHBrCIF, the difference between the full 1D and perturbed 1D approach is again negligible, whereas 2D contributions are significant.

A similar observation is also noticed for CHAtFI, which shows the largest absolute value of the PV vibrational frequency difference in the C-F stretching fundamental among the four halogenated methane derivatives discussed herein. This large shift is expected and mainly attributed to the presence of the heavier astatine nucleus. The full 1D and perturbative 1D treatment do not differ much. When taking the 2D terms into account, the values change significantly with the multi-mode contributions causing a reduction in absolute value compare to the perturbative 1D estimate of the frequency shift. This is expected to result from the fact, that the couplings of the C-F stretching mode v_4 to the C-H bending mode v_3 , where the frequencies are close ($\Delta\omega \approx 1.5\%$), and to the C-H stretching mode v_1 , where there is a factor of about three (≈ 2.9) between the fundamental frequencies are very strong. In the perturbative approach for LDA, even the sign and the order of magnitude of the effects for the fundamental transition (from $n_4 = 0$ to $n_4 = 1$) are altered.

Thus, the 2D perturbative terms are found to be important in all cases, which increase gradually for higher vibrational levels. Thus, the multi-mode effects due to the perturbative 2D approach increases the fundamental vibrational frequency shift for the CHBrCIF, CHClFI molecules whereas the shifts in CHBrFI molecule are lower in absolute value as compared to the perturbative 1D treatment counterparts. The heaviest At derivative shows the maximum frequency shift after the inclusion of the perturbative 2D effects at both HF and LDA level.

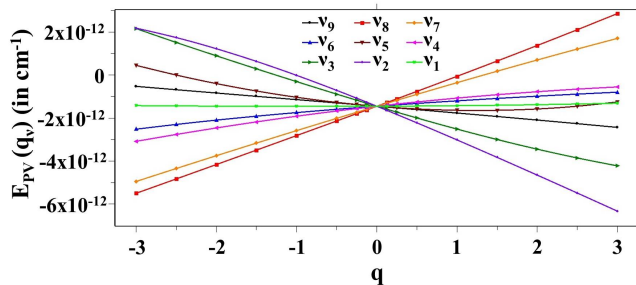


FIG. 5. HF parity-violating energy along the dimensionless reduced normal coordinates of CHBrCIF for all the normal modes.

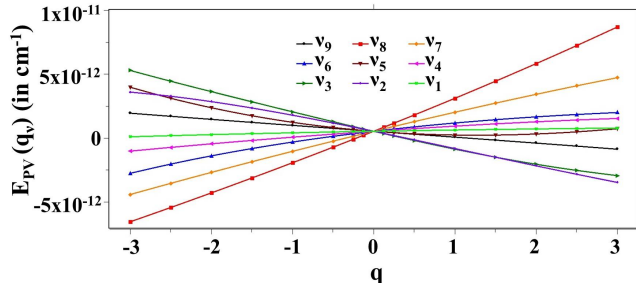


FIG. 6. LDA parity-violating energy along the dimensionless reduced normal coordinates of CHBrCIF for all the normal modes.

D. Multimode effects in CHBrCIF and CHAtFI

The influence of multi-mode effects^{53,87,88} from non-separable anharmonic effects have been estimated for CHBrCIF and the heaviest CHAtFI molecules after calculating the PV energy gradients along all the normal modes. Figures 5 and 6, respectively, display the variation of the HF and LDA PV energies along the dimensionless reduced normal coordinates of all the normal modes of CHBrCIF molecule. In both cases, normal coordinates q_8 , q_7 , q_3 and q_2 show steep slopes for the PV energy with respect to displacements along the respective dimensionless reduced normal coordinates. This may be naively expected, because the bending motion can alter the chiral structure of the molecule to a larger extent than a stretching vibration. In view of this, the vibrationally averaged PV potential has been computed along all the normal modes of CHBrCIF and the heavier CHAtFI analogue. Akin to the observation in CHBrCIF molecule, the bending vibrational modes in CHAtFI exhibit larger deviation in the PV energies as compared to other normal modes and hence, larger vibrational splittings and an enhancement of the perturbative 2D effects can be expected due to these modes.

Now, the vibrationally averaged HF and LDA PV gradients are utilised for calculating the 1D (Eq. 9) and 2D (Eq. 8) perturbative treatment for the vibrational energy levels up to 3rd vibrational states. For this purpose, in addition to the PV energy gradient $\vec{\nabla}E_{PV}$, which is available along all the normal modes, the second derivative (a_1 in Table II which is $\sim \frac{\partial^2 E_{PV}}{\partial q_i^2}$ in Eqs. 9 and 8) of the PV potential is needed. But it is not

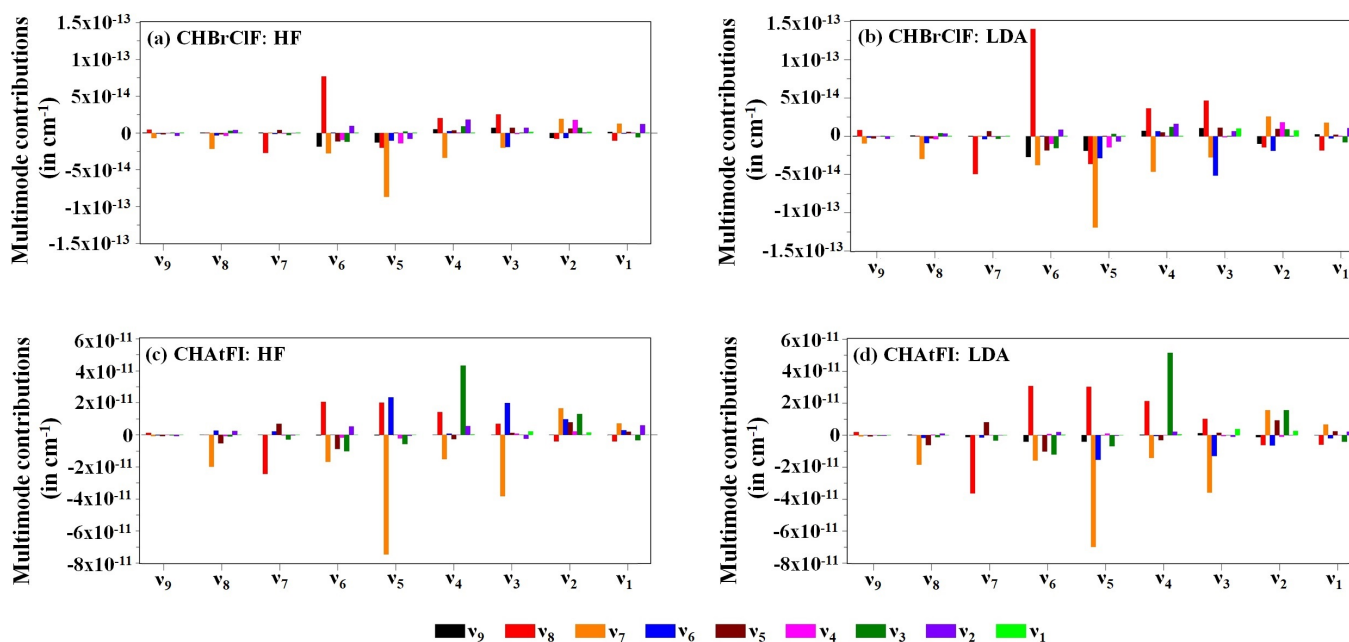


FIG. 7. Contributions (in cm^{-1}) to multi-mode effects from each of the normal coordinates to other fundamental vibrational transitions ($1 \leftarrow 0$) in the (S) -enantiomer of CHBrCIF and CHAtFI molecules at HF and LDA level of theory.

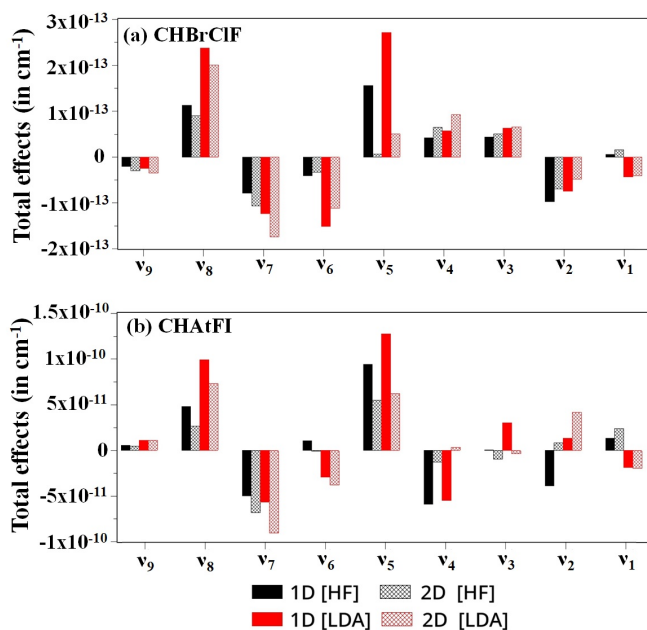


FIG. 8. 1D and 2D perturbative treatment of the vibrationally averaged HF and LDA parity-violating potential $E_{n,PV}^S$ leading to the shown PV frequency shifts (in cm^{-1}) for the fundamental transition ($1 \leftarrow 0$) in all the normal modes of the (S) -enantiomer of CHBrCIF and CHAtFI molecules.

necessary to compute a full profile, because with the availability of the analytic gradient, the second derivative (a_1) can be computed from the linear fit of only a few energy gradient points close to the equilibrium structure ($q = -0.125$ and

$q = 0.125$). This term is derived from a linear fit from these two points with another at $q = 0$ (cf. Tables S19-S20 in the Supporting Information).

The multi-mode contributions for the fundamental vibrational transition (from $n = 0$ to $n = 1$) for all the vibrational modes are estimated from Eq. 8. The q_8 , q_7 , q_3 and q_2 bending normal coordinates (although the corresponding fundamentals give rise to the least intense peaks in the infrared spectrum) contribute significantly to the multi-mode effects in the various fundamental transitions. Figure 7 displays the contributions towards the multi-mode effects for each of the vibrational modes of CHBrCIF and CHAtFI molecules at HF and LDA level of theory. Contributions from v_8 (in red) and v_7 (in orange) are the largest and they contribute to almost every fundamental, whereas q_6 and q_3 contribute moderately in CHBrCIF. The normal coordinate of the mode with the most intense fundamental in the vibrational spectrum, the C-F stretching fundamental (v_4), and other normal coordinates hardly contribute to multi-mode effects in other fundamentals. The observations are slightly different in CHAtFI. The contributions from q_8 (At-C-F bending in red) and q_7 (F-C-I bending in orange) normal coordinates are significant. In addition to this, the C-At stretching vibration (q_6) has shown a substantial contribution to the multi-mode effects. This is expected, as astatine is the heaviest nucleus of the molecule and, due to the steep Z -scaling of parity-violating effects, with Z being the nuclear charge, should also have a pronounced influence on the parity violating shifts. The C-F stretching fundamental (v_4) gets a large contributions from the H-C-F bending (q_3 in olive) normal coordinate, most probably due to the strong coupling between themselves since their frequencies are very close. Otherwise, the contributions from other vibrations are

not that significant.

The total observed shifts associated with the fundamental transition (from $n = 0$ to $n = 1$) for all the vibrational modes of the (*S*)-enantiomer of these two chiral derivatives from the 1D and 2D perturbative treatment are displayed in Figure 8. It should be noted that one needs to multiply these values by 2 and then divide by the vibrational frequencies of the corresponding fundamentals to get the relative PV vibrational frequency splittings between the C–F stretching fundamental of the *S*- and *R*-enantiomers of CHBrCIF and CHAtFI. The corresponding PV shifts up to the 3rd vibrational energy level as well as the PV shifts in the fundamental transitions (from $n = 0$ to $n = 1$) are included in Tables S25-S26 of the Supporting Information.

For CHBrCIF, the vibrational frequency shifts from the 1D perturbative treatment evaluated at HF level are larger in magnitude for ν_8 , ν_6 , ν_5 and ν_2 than that of the ν_4 C–F stretching mode. The steeper slope of the curves due to the large variation in the PV energies (which increases the numerical value of $\vec{\nabla}E_{PV}$) along q_8 , q_7 , q_3 and q_2 in Figure 5 favours these large vibrational shifts in the bending modes. On the other hand, the 2D perturbation results in large shifts for most modes as compared to the C–F stretching mode (ν_4). This is expected since the parity-violating multi-mode effects are significant in other bending modes and stretching modes other than the C–F stretching vibration (See Figure 7). From the comparison of 1D and 2D effects in frequency shifts within individual modes, it is found that the 2D effects increase the frequency shifts only in ν_9 , ν_7 , ν_4 and ν_3 , whereas other fundamentals follow the opposite trend (*cf.* Figure 8) where a cancellation of the 1D contribution is caused due to the 2D treatment. Total calculated PV shifts in the fundamentals transitions from both of the perturbative 1D and 2D treatments align either towards positive or negative directions. No alternation of the sign is observed even after adding multi-mode contributions to 1D perturbative ones. Overall, the estimated vibrational shift in all the fundamental transitions matches to the same order of magnitude of previous theoretical values.^{34,36}

The case for CHAtFI is slightly complicated. The 2D terms are important for all modes where ν_8 , ν_7 and ν_5 fundamentals show frequency shifts that are larger in absolute value as compared to the C–F stretching (ν_4) mode (*cf.* Figure 8). Multimode effects increase the frequency shifts by a factor of ~ 1.5 in ν_7 when compared to the perturbative 1D corrections. The correction due to multi-mode effects for the most intense C–F stretching mode reduces the absolute value as compared to the perturbative 1D result, i.e. the perturbative 2D treatment decreases the energy gap between the ground ($n = 0$) and 1st ($n = 1$) vibrational state. Even, as mentioned above (see Table IV), at LDA level the sign is altered (*cf.* Figure 8). A substantial increase in the ν_2 fundamental at LDA level is seen after including the multi-mode effects which is about 215% of the perturbative 1D value (See Figure 8). Although the fundamentals ν_8 and ν_5 have relatively larger frequency shifts for the vibrational transition from $n = 0$ to $n = 1$, the values decrease when multi-mode effects are introduced. Multimode contributions in ν_7 increases the frequency shifts in magnitude as compared to 1D effects. It may be noted that the asso-

ciated transition frequencies of these fundamentals are not in the range of the CO₂ laser used in the previous⁴² experimental set up. But, in spite of their lower intensity in the infrared spectrum, this might not be a severe limitation due to new developments in contemporary laser technology with quantum cascade laser being available in a broader frequency range.

We should emphasise, finally, that we reused in our present work the equilibrium structures and harmonic vibrational force fields from a previous study⁴⁰ to allow for direct comparison of results. Whereas a sophisticated CCSD(T) approach was used in Ref. 40, the basis sets were only of limited quality, which impacts not only on the equilibrium structures and harmonic force constants obtained, but also on the quality of molecular properties as was noted in our recent study⁸⁹ of nuclear electric quadrupole coupling constants in CHBrCIF and CHClFI. For CHBrCIF and its deuterated isotopomer, improved anharmonic ab initio force fields have been reported for instance in Ref. 90. In particular for the compound with the radioactive halogen, CHAtFI, for which no experimental information is available and for which very pronounced multi-mode effects on the C–F stretching fundamental were computed herein, a study with an improved description of the conventional parity-conserving effects is indicated. This becomes even more important by virtue of the potential role of heavy elemental chiral molecules in the search for dark matter candidates^{87,88} and recent advances in laser spectroscopy of radioactive molecules with short-lived nuclei.⁹¹

V. CONCLUDING REMARKS

In the present article, the gradient of the molecular parity-violating (PV) potential has been derived and implemented within a quasirelativistic framework at the level of HF and LDA, and is applied to rotational and vibrational spectroscopy of polyatomic molecules. A systematic study of frequency shifts in the rotational and vibrational spectra of chiral polyhalomethanes has been carried out.

A one-dimensional perturbative treatment has been compared to a previously calculated full anharmonic one-dimensional approach and found to be in good agreement. For the hypothetical astatine compound, the predicted frequency splitting is in the right order of magnitude to be measured when treating the problem in the one-dimensional approximation. The results form the multi-mode effects in CHBrCIF and CHAtFI reflects the importance of nonseparable anharmonic effects and suggests that the C–F stretching mode is not ideally suited for a measurement of electroweak PV effects, since other bending and stretching modes contribute significantly and can not be neglected. In view of this, choosing a proper vibrational transition is equally important as choosing a suitable molecule for conducting PV experiments and calculating the PV effects on the vibrational transition of chiral derivatives. Multimode effects are crucial for getting more insights about the vibrational transitions as well as rotational spectra in chiral compounds containing heavier atoms.

The present analytic derivative approach within a quasirelativistic mean-field scheme leads to an important simpli-

fication for routine calculation of PV frequency shift in rotational spectra of chiral molecules and of multi-mode contributions to the PV frequency shifts in rovibrational spectroscopy. The implementation of the analytic $\vec{\nabla}E_{\text{PV}}$ at other DFT levels such as GGA (e.g. BLYP) and GGA-based hybrid-functionals (e.g. B3LYP) is currently underway, which will increase its applicability to diverse chiral systems containing heavier nuclei, in particular transition metals. Also, such a development helps in measuring the functional dependencies and influence of electron correlation effects for the theoretical estimation of the PV effects in the rotational and vibrational transitions of chiral compounds. This will provide valuable information for future experiments aiming at the detection of molecular parity violation.

ACKNOWLEDGMENTS

The authors are particularly thankful to Yunlong Xiao, Sophie Nahrwold, Timur Isaev and Christoph van Wüllen for stimulating discussions. Financial support by the Deutsche Forschungsgemeinschaft (DFG, German Research Foundation) – Projektnummer 328961117 – SFB 1319 ELCH and the VolkswagenFoundation is gratefully acknowledged. The center for scientific computing (CSC) Frankfurt is thanked for computer time.

Appendix A: Variational Perturbation Theory

Following Refs. 56–58 the total energy $E(\vec{R}_0) = \langle \Psi | \hat{H}(\vec{R}_0) | \Psi \rangle$ parametrically depends on the nuclear coordinates. Within a mean-field approach, the energy satisfies

$$\vec{\nabla}_{\vec{t}} E(\vec{R}_0) = \vec{\nabla}_{\vec{t}} \langle \Psi(\vec{t}) | \hat{H}(\vec{R}_0) | \Psi(\vec{t}) \rangle = \vec{0}, \quad (\text{A1})$$

where \vec{t} is the vector of orbital rotations and $\vec{\nabla}_{\vec{t}}$ is the gradient with respect to \vec{t} . The variational energy of slightly displaced nuclei $E(\vec{R}_0 + \vec{\eta})$ can be expanded in a Taylor series in the nuclear displacements $\vec{\eta}$ as (see e.g. Ref. 59):

$$\begin{aligned} E(\vec{R}_0 + \vec{\eta}) &= E(\vec{R}_0) + \vec{\nabla}_{\vec{\eta}} E(\vec{R}_0 + \vec{\eta}) \Big|_{\vec{\eta}=\vec{0}} \cdot \vec{\eta} \\ &+ \frac{1}{2} \vec{\eta}^T \cdot \left[\vec{\nabla}_{\vec{\eta}} \otimes \vec{\nabla}_{\vec{\eta}} E(\vec{R}_0 + \vec{\eta}) \Big|_{\vec{\eta}=\vec{0}} \right] \cdot \vec{\eta} + \dots, \quad (\text{A2}) \end{aligned}$$

where $\vec{\nabla}_{\vec{\eta}}$ is the gradient with respect to the nuclear displacement vector.

Thus, the total variational energy is a function of λ_{PV} as well:

$$\begin{aligned} E_{\infty} &= E(\vec{R}_0 + \vec{\eta}, \lambda_{\text{PV}}) \\ &= E(\vec{R}_0 + \vec{\eta}) + \frac{\partial E(\vec{R}_0 + \vec{\eta}, \lambda_{\text{PV}})}{\partial \lambda_{\text{PV}}} \Big|_{\lambda_{\text{PV}}=0} \lambda_{\text{PV}} \\ &+ \frac{1}{2} \frac{\partial^2 E(\vec{R}_0 + \vec{\eta}, \lambda_{\text{PV}})}{\partial \lambda_{\text{PV}}^2} \Big|_{\lambda_{\text{PV}}=0} \lambda_{\text{PV}}^2 + \dots \quad (\text{A3}) \end{aligned}$$

In combination with Eq. (A2) the parity violating contribution $E_{\text{PV}}(\vec{R}_0 + \vec{\eta}, \lambda_{\text{PV}}) = E(\vec{R}_0 + \vec{\eta}, \lambda_{\text{PV}}) - E(\vec{R}_0)$ to the gradient of the energy with respect to nuclear displacements is:

$$\begin{aligned} \vec{\nabla}_{\vec{\eta}} E_{\text{PV}}(\vec{R}_0 + \vec{\eta}, \lambda_{\text{PV}}) \Big|_{\vec{\eta}=\vec{0}} &= \frac{\partial \vec{\nabla}_{\vec{\eta}} E(\vec{R}_0 + \vec{\eta}, \lambda_{\text{PV}})}{\partial \lambda_{\text{PV}}} \Big|_{\substack{\vec{\eta}=\vec{0} \\ \lambda_{\text{PV}}=0}} \lambda_{\text{PV}} \\ &+ \frac{1}{2} \frac{\partial^2 \vec{\nabla}_{\vec{\eta}} E(\vec{R}_0 + \vec{\eta}, \lambda_{\text{PV}})}{\partial \lambda_{\text{PV}}^2} \Big|_{\substack{\vec{\eta}=\vec{0} \\ \lambda_{\text{PV}}=0}} \lambda_{\text{PV}}^2 + \dots \\ &\approx \frac{\partial \vec{\nabla}_{\vec{\eta}} E(\vec{R}_0 + \vec{\eta}, \lambda_{\text{PV}})}{\partial \lambda_{\text{PV}}} \Big|_{\substack{\vec{\eta}=\vec{0} \\ \lambda_{\text{PV}}=0}} \lambda_{\text{PV}} \quad (\text{A4}) \end{aligned}$$

Appendix B: Spin polarised density functionals

We employ the approximation of non-collinear DFT. Then, we can write a exchange-correlation potential operator $\hat{V}_{\text{XC}}^{(\kappa)}$ as (see also Ref. 65)

$$\hat{V}_{\text{XC}}^{(\kappa)} = \hat{V}_{\text{XC,LDA}}^{(\kappa)} + \vec{V}_{\text{XC,GGA}}^{(\kappa)} \cdot \vec{\nabla}, \quad (\text{B1})$$

where $\vec{V}_{\text{XC,GGA}}^{(\kappa)} = \frac{\delta F_{\text{XC,GGA}}}{\delta \vec{\nabla} \rho_e^{(\kappa)}(\vec{r}; \mathbf{D}^{(\kappa)})}$ and for the explicit definitions of \vec{V}_{XC} see e.g. Refs. 63 and 65.

We define the spin or number density function $\rho_e^{(\kappa)}$ as

$$\rho_e^{(\kappa)}(\vec{r}; \mathbf{D}^{(\kappa)}) = \sum_{\mu\nu} \Re \left\{ D_{\mu\nu}^{(\kappa)} \right\} \chi_{\mu}(\vec{r}) \chi_{\nu}(\vec{r}). \quad (\text{B2})$$

Note, that this definition of the spin density coincides with what is usually called in non-collinear DFT the magnetization density and should not be confused with the length of the magnetization density which is what is called spin density in non-collinear DFT.

We can write the exchange-correlation energy as

$$E_{\text{XC}} = \sum_{\kappa} \sum_{\mu\nu} \Re D_{\mu\nu}^{(\kappa)} \langle \chi_{\mu} | \hat{V}_{\text{XC}}^{(\kappa)} | \chi_{\nu} \rangle \quad (\text{B3})$$

and the gradient with respect to nuclear displacements is

$$\vec{\nabla}_{\vec{\eta}} E_{\text{XC}} = 2 \sum_{\kappa} \sum_{\mu\nu} \Re D_{\mu\nu}^{(\kappa)} \langle \vec{\nabla}_{\vec{\eta}} \chi_{\mu} | \hat{V}_{\text{XC}}^{(\kappa)} | \chi_{\nu} \rangle. \quad (\text{B4})$$

In presence of a perturbing operator such as the parity-violating potential we have to compute the first order perturbed exchange-correlation potential operator as

$$\begin{aligned} \hat{V}_{\text{XC}}'^{(\kappa)} &= \sum_{\lambda} \frac{\delta \hat{V}_{\text{XC}}^{(\kappa)}}{\delta \rho_e^{(\lambda)}(\vec{r}; \mathbf{D}^{(\lambda)})} \rho_e^{(\lambda)}(\vec{r}; \mathbf{D}^{(\lambda)}) \\ &+ \sum_{\lambda} \frac{\delta \hat{V}_{\text{XC}}^{(\kappa)}}{\delta \vec{\nabla} \rho_e^{(\lambda)}(\vec{r}; \mathbf{D}^{(\lambda)})} \vec{\nabla} \rho_e^{(\lambda)}(\vec{r}; \mathbf{D}^{(\lambda)}), \quad (\text{B5}) \end{aligned}$$

where $\rho_e^{(\kappa)}(\vec{r}; \mathbf{D}^{(\kappa)})$ is the perturbed density function of first order in λ_{PV} .

Appendix C: Nuclear displacement gradient of a first order property

$$\mathbf{h}_{\text{ZORA}}^{(\kappa)} + \mathbf{h}_{\text{PV}}^{(\kappa)} + \mathbf{G}^{(\kappa)}(\mathbf{D}^\infty)$$

We can express terms that are proportional to gradients of the density matrix in terms of the Fock matrix $\mathbf{F}^{(\kappa)}(\mathbf{D}^\infty) =$

$$\vec{\nabla}_{\vec{\eta}} E_\infty = \Re \left\{ \sum_{\mu\nu} \left[\sum_{\kappa=0}^3 D_{\mu\nu}^{\infty,(\kappa)} \left(\vec{\nabla}_{\vec{\eta}} h_{\text{ZORA},\mu\nu}^{(\kappa)} \right) + \frac{1}{2} \sum_{\kappa=0}^3 D_{\mu\nu}^{\infty,(\kappa)} \vec{G}_{\text{grad},\mu\nu}^{(\kappa)}(\mathbf{D}^\infty) + \sum_{\kappa=1}^3 D_{\mu\nu}^{\infty,(\kappa)} \left(\vec{\nabla}_{\vec{\eta}} h_{\text{PV},\mu\nu}^{(\kappa)} \right) + \sum_{\kappa=0}^3 \left(\vec{\nabla}_{\vec{\eta}} D_{\mu\nu}^{\infty,(\kappa)} \right) F_{\mu\nu}^{(\kappa)}(\mathbf{D}^\infty) \right] \right\}, \quad (\text{C1})$$

where we have defined the matrix $\vec{G}_{\text{grad}}^{(\kappa)}$ of contracted gradients of two-electron integrals with elements:

$$\vec{G}_{\text{grad},\mu\nu}^{(\kappa)}(\mathbf{D}) = \sum_{\rho\sigma} \left[\delta_{\kappa 0} D_{\rho\sigma}^{(\kappa)} \vec{\nabla}_{\vec{\eta}} (\mu\nu|\rho\sigma) - a_X \frac{1}{2} D_{\rho\sigma}^{(\kappa)} \vec{\nabla}_{\vec{\eta}} (\mu\sigma|\rho\nu) + 2a_{\text{DFT}} \left\langle \vec{\nabla}_{\vec{\eta}} \chi_\mu \left| V_{\text{XC}}^{(\kappa)}(\mathbf{D}) \right| \chi_\nu \right\rangle \right]. \quad (\text{C2})$$

The canonical SCF equations are

$$\mathbf{FC} = \mathbf{SC}\varepsilon; \quad \mathbf{C}^\dagger \mathbf{SC} = \mathbf{1}, \quad (\text{C3})$$

where $\mathbf{S} = \sigma^0 \otimes \mathbf{S}_{1c}$ is the overlap matrix constructed from the one component overlap matrix \mathbf{S}_{1c} of the basis functions and $\mathbf{F} = \sum_{\kappa=0}^3 \sigma^\kappa \otimes \mathbf{F}^{(\kappa)}(\mathbf{D})$. The matrix of coefficients is chosen as

$$\mathbf{C} = \begin{pmatrix} \mathbf{C}^{(\alpha)} \\ \mathbf{C}^{(\beta)} \end{pmatrix}. \quad (\text{C4})$$

Exploiting the Hermiticity of \mathbf{F} and ε we find from this

$$(\vec{\nabla}_{\vec{\eta}} \mathbf{C}^\dagger) \mathbf{FC} + \mathbf{C}^\dagger \mathbf{F} (\vec{\nabla}_{\vec{\eta}} \mathbf{C}) = (\vec{\nabla}_{\vec{\eta}} \mathbf{C}^\dagger) \mathbf{SC}\varepsilon + \varepsilon \mathbf{C}^\dagger \mathbf{S} (\vec{\nabla}_{\vec{\eta}} \mathbf{C}) \quad (\text{C5})$$

Furthermore, the gradient of the orthonormality condition in Eq. C3 gives

$$(\vec{\nabla}_{\vec{\eta}} \mathbf{C}^\dagger) \mathbf{SC} + \mathbf{C}^\dagger \mathbf{S} (\vec{\nabla}_{\vec{\eta}} \mathbf{C}) = -\mathbf{C}^\dagger (\vec{\nabla}_{\vec{\eta}} \mathbf{S}) \mathbf{C} \quad (\text{C6})$$

Therewith, the contribution to the energy gradient from the Fock matrix in Eq. (C1) can be expressed via the orthonormality condition as

$$\begin{aligned} \sum_{\mu\nu} \sum_{\kappa=0}^3 \left(\vec{\nabla}_{\vec{\eta}} D_{\mu\nu}^{\infty,(\kappa)} \right) F_{\mu\nu}^{(\kappa)}(\mathbf{D}^\infty) &= \sum_{\mu\nu} \sum_i n_i \sum_{\kappa=0}^3 \left[(\vec{\nabla}_{\vec{\eta}} \vec{C}_{\mu i}^\infty)^\dagger \sigma^{(\kappa)} F_{\mu\nu}^{(\kappa)}(\mathbf{D}^\infty) \vec{C}_{\nu i}^\infty + (\vec{C}_{\mu i}^\infty)^\dagger \sigma^{(\kappa)} F_{\mu\nu}^{(\kappa)}(\mathbf{D}^\infty) (\vec{\nabla}_{\vec{\eta}} \vec{C}_{\nu i}^\infty) \right] \\ &= \sum_{\mu\nu} \sum_i n_i \varepsilon_i^\infty \left[(\vec{\nabla}_{\vec{\eta}} \vec{C}_{\mu i}^\infty)^\dagger S_{\mu\nu} \vec{C}_{\nu i}^\infty + (\vec{C}_{\mu i}^\infty)^\dagger S_{\mu\nu} (\vec{\nabla}_{\vec{\eta}} \vec{C}_{\nu i}^\infty) \right] \\ &= -\sum_{\mu\nu} \sum_i n_i \varepsilon_i^\infty (\vec{C}_{\mu i}^\infty)^\dagger (\vec{\nabla}_{\vec{\eta}} S_{\mu\nu}) \vec{C}_{\nu i}^\infty \\ &= -\sum_{\mu\nu} W_{\mu\nu}^{\infty,(0)} \vec{\nabla}_{\vec{\eta}} S_{\mu\nu} \end{aligned} \quad (\text{C7})$$

where we introduced the energy weighted density matrix (EWDM) \mathbf{W} as

$$\mathbf{W}^{(\kappa)} = \sum_{i=1}^{N_{\text{orb}}} n_i \varepsilon_i \mathbf{D}_i^{(\kappa)}. \quad (\text{C8})$$

Appendix D: Linear response equations

1. First order perturbed density matrix

The infinite order coefficients can be expressed in terms of orbital rotations, expressed via the anti-Hermitian matrix \mathbf{T}_∞

as

$$\mathbf{C}^\infty = \mathbf{C}_0 \mathbf{e}^{\mathbf{T}_\infty} \quad (\text{D1})$$

were \mathbf{C}_0 is the initial guess of orthonormal orbitals and $(\mathbf{C}^\infty)^\dagger = \mathbf{e}^{-\mathbf{T}_\infty} \mathbf{C}_0^\dagger$. From the definition of the density matrix [Eq. (18)] we see $\mathbf{D}^\infty = (\mathbf{C}^\infty \mathbf{N} (\mathbf{C}^\infty)^\dagger)^\top = (\mathbf{C}^\infty)^* \mathbf{N} (\mathbf{C}^\infty)^\top$, where \mathbf{N} is a diagonal matrix containing the occupation numbers n_i . Thus, the perturbed density matrix of infinite order \mathbf{D}^∞ can be written in terms of orbital rotation matrix \mathbf{T}_∞ as

$$\mathbf{D}^\infty = \mathbf{C}_0^* \mathbf{e}^{-\mathbf{T}_\infty^\top} \mathbf{N} \mathbf{e}^{\mathbf{T}_\infty} \mathbf{C}_0^\top. \quad (\text{D2})$$

Moreover, we can write \mathbf{D}^∞ in terms of the unperturbed orbital coefficients \mathbf{C} , received from orbital rotations \vec{l}_0 in absence of the perturbation with the corresponding rotation matrix \mathbf{T}_0 and an the rotation matrix \mathbf{T} as:

$$\mathbf{D}^\infty = \mathbf{C}_0^* \mathbf{e}^{-\mathbf{T}_0^\top} \mathbf{e}^{-\mathbf{T}^\top} \mathbf{N} \mathbf{e}^{\mathbf{T}} \mathbf{e}^{\mathbf{T}_0} \mathbf{C}_0^\top = \mathbf{C}^* \mathbf{e}^{-\mathbf{T}^\top} \mathbf{N} \mathbf{e}^{\mathbf{T}} \mathbf{C}^\top. \quad (\text{D3})$$

When assuming \mathbf{N} to be successively sorted for occupied and unoccupied orbitals we can write the transformation matrix \mathbf{T} in blocked form as

$$\mathbf{T} = \begin{pmatrix} \mathbf{T}_{oo} & -\mathbf{T}_{uo}^\dagger \\ \mathbf{T}_{uo} & \mathbf{T}_{uu} \end{pmatrix}, \quad (\text{D4})$$

where, o means occupied and u means unoccupied. In first order the perturbed density matrix can be written in terms of the unoccupied-occupied block \mathbf{T}_{uo} of \mathbf{T} :

$$\begin{aligned} \mathbf{D}' &= \mathbf{C}^* (\mathbf{N} \mathbf{T}^\top - \mathbf{T}^\top \mathbf{N}) \mathbf{C}^\top \\ &= \mathbf{C}^* (\mathbf{N} \mathbf{T}^\top + \mathbf{T}^* \mathbf{N}) \mathbf{C}^\top \\ &= \mathbf{C}^* \begin{pmatrix} \mathbf{0} & \mathbf{T}_{uo}^\top \\ \mathbf{T}_{uo}^* & \mathbf{0} \end{pmatrix} \mathbf{C}^\top. \end{aligned} \quad (\text{D5})$$

Thus, we arrive at

$$D'_{\mu\nu}{}^{(\kappa)}(\mathbf{T}_{uo}) = \sum_i^{\text{occ}} \sum_a^{\text{unocc}} \left[\vec{C}_{\mu a}^{\dagger} \sigma^{(\kappa)} \vec{C}_{\nu i} T_{ai}^* + \vec{C}_{\nu i}^{\dagger} \sigma^{(\kappa)} \vec{C}_{\mu a} T_{ai} \right]. \quad (\text{D6})$$

2. Coupled perturbed HF/KS equations

The coupled perturbed HF (CPHF) or coupled perturbed KS (CPKS) equations read (see Ref. 69).

$$\mathbf{F} \mathbf{C}' + \mathbf{F}' \mathbf{C} = \mathbf{S}' \mathbf{C} \varepsilon + \mathbf{S} \mathbf{C}' \varepsilon + \mathbf{S} \mathbf{C} \varepsilon' \quad (\text{D7})$$

where, a prime denotes matrices linear in λ_{PV} and unprimed matrices are unperturbed ($\lambda_{\text{PV}} = 0$). The perturbed Fock matrix \mathbf{F}' is for perturbation independent basis functions as we have in the case of the perturbation due to the PV potential:

$$F'_{\mu\nu} = \sum_{\kappa} \sigma^{\kappa} h_{\text{PV},\mu\nu}^{(\kappa)} + \sigma^{\kappa} G_{\mu\nu}^{(\kappa)}(\mathbf{D}'(\mathbf{T}_{uo})) \quad (\text{D8})$$

where, we introduced the self consistent transformation matrix of the orbital coefficients \mathbf{T} for which $\mathbf{C}' = \mathbf{C} \mathbf{T}$. From

Eq. (D5) we see that only the unoccupied-occupied rotations change the orbitals in first order, such that we can focus on the of unoccupied-occupied block of Eq (D7). Thus, for perturbation independent basis functions the CPHF/CPKS equations reduce to the coupled equations

$$\varepsilon_u \mathbf{T}_{uo} + \mathbf{C}_u^\dagger \mathbf{F}' \mathbf{C}_o = \mathbf{T}_{uo} \varepsilon_o \quad (\text{D9})$$

$$\varepsilon_o \mathbf{T}_{ou} + \mathbf{C}_o^\dagger \mathbf{F}' \mathbf{C}_u = \mathbf{T}_{ou} \varepsilon_u, \quad (\text{D10})$$

with the unoccupied (u) and occupied (o) orbital sub-blocks of \mathbf{C} and ε . From this, one arrives at the linear response equations (see e.g. Refs. 70 and 71)

$$\sum_{bj} \begin{pmatrix} \mathbf{A}_{bj} & \mathbf{B}_{bj} \\ \mathbf{B}_{bj}^* & \mathbf{A}_{bj}^* \end{pmatrix} \begin{pmatrix} T_{bj} \\ h T_{bj}^* \end{pmatrix} = - \begin{pmatrix} \mathbf{H}_{\text{PV},\text{MO}}^{\text{uo}} \\ \mathbf{H}_{\text{PV},\text{MO}}^{\text{uo}*} \end{pmatrix}, \quad (\text{D11})$$

where the index b runs over unoccupied orbitals and the index j runs over occupied orbitals. The Hermiticity factor h results from the orthonormality condition which for perturbation independent basis functions yields $\mathbf{C}^\dagger \mathbf{S} \mathbf{C} \mathbf{T} = -\mathbf{T}^\dagger \mathbf{C}^\dagger \mathbf{S} \mathbf{C} \Leftrightarrow \mathbf{T}^\dagger = -\mathbf{T}$, which is in accordance with Eq. (D2). For observables such as \mathbf{H}_{PV} we have $h = +1$.

¹C. S. Wu, E. Ambler, R. W. Hayward, D. D. Hoppes, and R. P. Hudson, "Experimental test of parity conservation in beta decay," *Phys. Rev.* **105**, 1413–1415 (1957).

²T. D. Lee and C. N. Yang, "Question of parity conservation in weak interactions," *Phys. Rev.* **104**, 254–258 (1956).

³Y. Yamagata, "A hypothesis for the asymmetric appearance of biomolecules on earth," *J. Theor. Biol.* **11**, 495–498 (1966).

⁴É. Gajzágó and G. Marx, "Energy difference of mirror molecules," *Atomki Köz. Suppl.* **16**, 177–184 (1974).

⁵V. S. Letokhov, "On difference of energy levels of left and right molecules due to weak interactions," *Phys. Lett. A* **53**, 275–276 (1975).

⁶B. Y. Zel'dovich, D. B. Saakyan, and I. I. Sobel'man, "Energy difference between right-hand and left-hand molecules, due to parity nonconservation in weak interactions of electrons with nuclei," *JETP Lett.* **25**, 94–97 (1977).

⁷B. Y. Zel'dovich, D. B. Saakyan, and I. I. Sobel'man, "Energy difference between right-hand and left-hand molecules, due to parity nonconservation in weak interactions of electrons with nuclei," *Pis'ma Zhurnal Eksperimentalnoi I Teoreticheskoi Fiziki* **25**, 106–109 (1977).

⁸R. A. Hegstrom, D. W. Rein, and P. G. H. Sanders, "Calculation of the parity nonconserving energy difference between mirror-image molecules," *J. Chem. Phys.* **73**, 2329–2341 (1980).

⁹I. B. Khriplovich, "On the energy difference between optical isomers resulting from parity nonconservation," *Sov. Phys. JETP* **52**, 177–183 (1980).

¹⁰V. G. Gorshkov, M. G. Kozlov, and L. N. Labzovsky, "P-odd effects in polyatomic molecules," *Zhurnal Eksperimentalnoi I Teoreticheskoi Fiziki* **82**, 1807–1819 (1982).

¹¹V. G. Gorshkov, M. G. Kozlov, and L. N. Labzovsky, "P-odd effects in polyatomic molecules," *Sov. Phys. JETP* **55**, 1042–1048 (1982).

¹²M. Quack, "On the measurement of the parity violating energy difference between enantiomers," *Chem. Phys. Lett.* **132**, 147–153 (1986).

¹³R. N. Compton and R. M. Pagni, "The chirality of biomolecules," *Advances In Atomic, Molecular, And Optical Physics*, Vol 48 **48**, 219–261 (2002).

¹⁴O. N. Kompanets, A. R. Kukudzhanov, V. S. Letokhov, and L. L. Gervits, "Narrow resonances of saturated absorption of the asymmetrical molecule CHFClBr and the possibility of weak current detection in molecular physics," *Opt. Commun.* **19**, 414–416 (1976).

¹⁵E. Arimondo, P. Glorieux, and T. Oka, "Observation of inverted infrared lamb dips in separated optical isomers," *Opt. Commun.* **23**, 369–372 (1977).

¹⁶A. Bauder, A. Beil, D. Luckhaus, F. Müller, and M. Quack, "Combined high resolution infrared and microwave study of bromochloroformethane," *J. Chem. Phys.* **106**, 7558–7570 (1997).

- ¹⁷C. Daussy, T. Marrel, A. Amy-Klein, C. T. Nguyen, C. J. Bordé, and C. Chardonnet, "Limit on the parity nonconserving energy difference between the enantiomers of a chiral molecule by laser spectroscopy," *Phys. Rev. Lett.* **83**, 1554–1557 (1999).
- ¹⁸R. A. Harris and L. Stodolski, "The effect of the parity violating electron-nucleus interaction on the spin-spin coupling Hamiltonian of chiral molecules," *J. Chem. Phys.* **73**, 3862–3863 (1980).
- ¹⁹M. Schnell and J. Küpper, "Tailored molecular samples for precision spectroscopy experiments," *Faraday Disc.* **150**, 33–49 (2011).
- ²⁰A. L. Barra, J. B. Robert, and L. Wiesenfeld, "Parity non-conservation and NMR observables. Calculation of T1 resonance frequency differences in enantiomers," *Phys. Lett. A* **115**, 443–447 (1986).
- ²¹A. L. Barra, J. B. Robert, and L. Wiesenfeld, "Possible observation of parity nonconservation by high-resolution NMR," *Europhys. Lett.* **5**, 217–222 (1988).
- ²²A. L. Barra and J. B. Robert, "Parity non-conservation and NMR parameters," *Mol. Phys.* **88**, 875–886 (1996).
- ²³J. Eills, J. W. Blanchard, L. Bougas, M. G. Kozlov, A. Pines, and D. Budker, "Measuring molecular parity nonconservation using nuclear-magnetic-resonance spectroscopy," *Phys. Rev. A* **96**, 042119 (2017).
- ²⁴R. A. Harris and L. Stodolski, "Quantum beats in optical activity and weak interactions," *Phys. Lett. B* **78**, 313–317 (1978).
- ²⁵R. A. Harris and L. Stodolski, "On the time dependence of optical activity," *J. Chem. Phys.* **74**, 2145–2155 (1981).
- ²⁶R. Berger, "Molecular parity violation in electronically excited states," *Phys. Chem. Chem. Phys.* **5**, 12–17 (2003).
- ²⁷M. Quack, "Structure and dynamics of chiral molecules," *Angew. Chem. Int. Ed.* **28**, 571–586 (1989).
- ²⁸M. Quack, "How important is parity violation for molecular and biomolecular chirality?" *Angew. Chem. Int. Ed.* **41**, 4618–4630 (2002).
- ²⁹R. Berger, "Parity-violation effects in molecules," in *Relativistic Electronic Structure Theory, Part: 2, Applications*, edited by P. Schwerdtfeger (Elsevier, Netherlands, 2004) Chap. 4, pp. 188–288.
- ³⁰J. Crassous, C. Chardonnet, T. Saue, and P. Schwerdtfeger, "Recent experimental and theoretical developments towards the observation of parity violation (pv) effects in molecules by spectroscopy," *Org. Biomol. Chem.* **3**, 2218–2224 (2005).
- ³¹M. Quack, J. Stohner, and M. Willeke, "High-resolution spectroscopic studies and theory of parity violation in chiral molecules," *Annu. Rev. Phys. Chem.* **59**, 741–769 (2008).
- ³²P. Schwerdtfeger, "The search for parity violation in chiral molecules," in *Computational Spectroscopy: Methods, Experiments and Applications*, edited by J. Grunenberg (Wiley, Netherlands, 2010) Chap. 7, pp. 201–221.
- ³³R. Berger and J. Stohner, "Parity violation," *Wiley Interdiscip. Rev.-Comput. Mol. Sci.* **9**, e1396 (2019), <https://onlinelibrary.wiley.com/doi/pdf/10.1002/wcms.1396>.
- ³⁴M. Quack and J. Stohner, "Influence of parity violating weak nuclear potentials on vibrational and rotational frequencies in chiral molecules," *Phys. Rev. Lett.* **84**, 3807–3810 (2000).
- ³⁵J. K. Laerdahl and P. Schwerdtfeger and H. M. Quiney, "Theoretical analysis of parity-violating energy differences between the enantiomers of chiral molecules," *Phys. Rev. Lett.* **84**, 3811–3814 (2000).
- ³⁶R. G. Vigiore, R. Zanasi, P. Lazzaretti, and A. Ligabue, "Theoretical determination of parity-violating vibrational frequency differences between the enantiomers of the CHFClBr molecule," *Phys. Rev. A* **62**, 052516 (2000).
- ³⁷M. Quack and J. Stohner, "How do parity violating weak nuclear interactions influence rovibrational frequencies in chiral molecules?" *Z. Phys. Chem.* **214**, 675–703 (2000).
- ³⁸P. Schwerdtfeger, J. K. Laerdahl, and C. Chardonnet, "Calculation of parity-violating effects for the C-F stretching mode of chiral methyl fluorides," *Phys. Rev. A* **65**, 042508 (2002).
- ³⁹M. Quack and J. Stohner, "Parity violation in chiral molecules," *Chimia* **59**, 530–538 (2005).
- ⁴⁰R. Berger and J. L. Stuber, "Electroweak interactions in chiral molecules: Two-component density functional theory study of vibrational frequency shifts in polyhalomethanes," *Mol. Phys.* **105**, 41–49 (2007).
- ⁴¹C. Thierfelder, G. Rauhut, and P. Schwerdtfeger, "Relativistic coupled-cluster study of the parity-violation energy shift of chfclbr," *Phys. Rev. A* **81**, 032513 (2010).
- ⁴²M. Ziskind, C. Daussy, T. Marrel, and C. Chardonnet, "Improved sensitivity in the search for a parity-violating energy difference in the vibrational spectrum of the enantiomers of CHFClBr," *Eur. Phys. J. D* **20**, 219–225 (2002).
- ⁴³B. Darquie, C. Stoeffler, A. Shelkovnikov, C. Daussy, A. Amy-Klein, C. Chardonnet, S. Zrig, L. Guy, J. Crassous, P. Soulard, P. Asselin, T. R. Huet, P. Schwerdtfeger, R. Bast, and T. Saue, "Progress Toward the First Observation of Parity Violation in Chiral Molecules by High-Resolution Laser Spectroscopy," *Chirality* **22**, 870–884 (2010).
- ⁴⁴A. Cournol, M. Manceau, M. Pierens, L. Lecordier, D. B. A. Tran, R. Santagata, B. Argence, A. Goncharov, O. Lopez, M. Abgrall, Y. L. Coq, R. L. Targat, H. A. Martinez, W. K. Lee, D. Xu, P. E. Pottie, R. J. Hendricks, T. E. Wall, J. M. Bieniewska, B. E. Sauer, M. R. Tarbutt, A. Amy-Klein, S. K. Tokunaga, and B. Darquie, "A new experiment to test parity symmetry in cold chiral molecules using vibrational spectroscopy," *Quantum Electron.* **49**, 288–292 (2019).
- ⁴⁵F. Faglioni and P. Lazzaretti, "Parity violation effect on vibrational spectra," *Phys. Rev. A* **67**, 032101 (2003).
- ⁴⁶P. Schwerdtfeger, J. Gierlich, and T. Bollwein, "Large parity-violation effects in heavy-metal-containing chiral compounds," *Angew. Chem. Int. Ed.* **42**, 1293–1296 (2003).
- ⁴⁷R. Bast and P. Schwerdtfeger, "Parity-violation effects in the C-F stretching mode of heavy-atom methyl fluorides," *Phys. Rev. Lett.* **91**, 023001 (2003).
- ⁴⁸A. Messiah, *Quantenmechanik*, Vol. 1 (Walter de Gruyter, Berlin, 1976).
- ⁴⁹T. Marrel, M. Ziskind, C. Daussy, and C. Chardonnet, "High precision rovibrational and hyperfine analysis of the $v_4 = 1$ level of bromochlorofluoromethane," *J. Mol. Struct.* **599**, 195–209 (2001).
- ⁵⁰J. K. Laerdahl, R. Wesendrup, and P. Schwerdtfeger, "Parity-violating interactions and biochemical homochirality," *ChemPhysChem* **1**, 60–62 (2000).
- ⁵¹M. Quack and J. Stohner, "Molecular chirality and the fundamental symmetries of physics: Influence of parity violation on rovibrational frequencies and thermodynamic properties," *Chirality* **13**, 745–753 (2001).
- ⁵²P. Schwerdtfeger, T. Saue, J. N. P. van Stralen, and L. Visscher, "Relativistic second-order many-body and density-functional theory for the parity-violation contribution to the C-F stretching mode in CHFClBr," *Phys. Rev. A* **71**, 012103 (2005).
- ⁵³M. Quack and J. Stohner, "Combined multidimensional anharmonic and parity violating effects in cdbrcf," *J. Chem. Phys.* **119**, 11228–11240 (2003).
- ⁵⁴G. Rauhut, "Efficient calculation of potential energy surfaces for the generation of vibrational wave functions," *J. Chem. Phys.* **121**, 9313–9322 (2004), <https://doi.org/10.1063/1.1804174>.
- ⁵⁵A. D. Buckingham and W. Urland, "Isotope effects on molecular properties," *Chem. Rev.* **75**, 113–117 (1975), <https://doi.org/10.1021/cr60293a005>.
- ⁵⁶D. Jayatilaka, P. E. Maslen, R. D. Amos, and N. C. Handy, "Higher analytic derivatives," *Mol. Phys.* **75**, 271–291 (1992), <https://doi.org/10.1080/00268979200100221>.
- ⁵⁷R. Bast, U. Ekström, B. Gao, T. Helgaker, K. Ruud, and A. J. Thorvaldsen, "The ab initio calculation of molecular electric, magnetic and geometric properties," *Phys. Chem. Chem. Phys.* **13**, 2627–2651 (2011).
- ⁵⁸T. Helgaker, S. Coriani, P. Jørgensen, K. Kristensen, J. Olsen, and K. Ruud, "Recent advances in wave function-based methods of molecular-property calculations," *Chem. Rev.* **112**, 543–631 (2012), PMID: 22236047, <https://doi.org/10.1021/cr2002239>.
- ⁵⁹H. Sellers, "Variational energy derivatives and perturbation theory," *Int. J. Quantum Chem.* **33**, 271–277 (1988), <https://onlinelibrary.wiley.com/doi/pdf/10.1002/qua.560330403>.
- ⁶⁰C. Chang, M. Pelissier, and P. Durand, "Regular two-component Pauli-like effective Hamiltonians in Dirac theory," *Phys. Scr.* **34**, 394–404 (1986).
- ⁶¹E. van Lenthe, J. G. Snijders, and E.-J. Baerends, "The zero-order regular approximation for relativistic effects: The effect of the spin-orbit coupling in closed shell molecules," *J. Chem. Phys.* **105**, 6505 (1996).
- ⁶²C. van Wüllen, "Molecular density functional calculations in the regular relativistic approximation: Method, application to coinage metal diatomics, hydrides, fluorides and chlorides, and comparison with first-order relativistic calculations," *J. Chem. Phys.* **109**, 392–399 (1998).
- ⁶³C. van Wüllen, "A Quasirelativistic Two-component Density Functional and Hartree-Fock Program," *Z. Phys. Chem* **224**, 413–426 (2010).

- ⁶⁴R. Berger, N. Langermann, and C. van Wüllen, “Zeroth order regular approximation approach to molecular parity violation,” *Phys. Rev. A* **71**, 042105 (2005).
- ⁶⁵C. van Wüllen and N. Langermann, “Gradients for two-component quasirelativistic methods. application to dihalogenides of element 116,” *J. Chem. Phys.* **126**, 114106 (2007), <https://doi.org/10.1063/1.2711197>.
- ⁶⁶O. Treutler and R. Ahlrichs, “Efficient molecular numerical integration schemes,” *J. Chem. Phys.* **102**, 346 (1995).
- ⁶⁷A. D. Becke, “Density-functional exchange-energy approximation with correct asymptotic-behavior,” *Phys. Rev. A* **38**, 3098–3100 (1988).
- ⁶⁸M. Ringholm, D. Jonsson, and K. Ruud, “A general, recursive, and open-ended response code,” *J. Comput. Chem.* **35**, 622–633 (2014).
- ⁶⁹J. Olsen, D. L. Yeager, and P. Jørgensen, “Triplet excitation properties in large scale multiconfiguration linear response calculations,” *J. Chem. Phys.* **91**, 381–388 (1989).
- ⁷⁰P. Sałek, O. Vahtras, T. Helgaker, and H. Ågren, “Density-functional theory of linear and nonlinear time-dependent molecular properties,” *J. Chem. Phys.* **117**, 9630–9645 (2002), <https://doi.org/10.1063/1.1516805>.
- ⁷¹T. Saue and H. J. A. Jensen, “Linear response at the 4-component relativistic level: Application to the frequency-dependent dipole polarizabilities of the coinage metal dimers,” *J. Chem. Phys.* **118**, 522–536 (2003), <https://doi.org/10.1063/1.1522407>.
- ⁷²S. Nahrwold and R. Berger, “Zeroth order regular approximation approach to parity violating nuclear magnetic resonance shielding tensors,” *J. Chem. Phys.* **130**, 214101 (2009).
- ⁷³T. A. Isaev and R. Berger, “Electron correlation and nuclear charge dependence of parity-violating properties in open-shell diatomic molecules,” *Phys. Rev. A* **86**, 062515 (2012).
- ⁷⁴M. Häser and R. Ahlrichs, “Improvements on the direct SCF method,” *J. Comput. Chem.* **10**, 104–111 (1989).
- ⁷⁵R. Ahlrichs, M. Bär, M. Häser, H. Horn, and C. Kölmel, “Electronic structure calculations on workstation computers: The program system turbomole,” *Chem. Phys. Lett.* **162**, 165–169 (1989).
- ⁷⁶MATLAB, 9.7.0.1190202 (R2019b) (The MathWorks Inc., Natick, Massachusetts, 2018).
- ⁷⁷K. Gaul and R. Berger, “Toolbox approach for quasi-relativistic calculation of molecular properties for precision tests of fundamental physics,” *J. Chem. Phys.* **152**, 044101 (2020), [arXiv:1907.10432 \[physics.chem-ph\]](https://arxiv.org/abs/1907.10432).
- ⁷⁸V. Barone and R. G. Viglione, “Harmonic and anharmonic contributions to parity-violating vibrational frequency difference between enantiomers of chiral molecules,” *J. Chem. Phys.* **123**, 234304 (2005), <https://doi.org/10.1063/1.2137719>.
- ⁷⁹A. Bergner, M. Dolg, W. Küchle, H. Stoll, and H. Preuß, “*Ab initio* energy-adjusted pseudopotentials for elements of groups 13–17,” *Mol. Phys.* **80**, 1431–1441 (1993).
- ⁸⁰W. Küchle, M. Dolg, H. Stoll, and H. Preuss, “*Ab initio* pseudopotentials for Hg through Rn I. parameter sets and atomic calculations,” *Mol. Phys.* **74**, 1245–1263 (1991).
- ⁸¹H.-J. Werner, P. J. Knowles, G. Knizia, F. R. Manby, and M. Schütz, “no title,” *WIREs Comput. Mol. Sci.* **2**, 242–253 (2012).
- ⁸²Q. Ma and H.-J. Werner, “Explicitly correlated local coupled-cluster methods using pair natural orbitals,” *WIREs Comput. Mol. Sci.* **8**, e1371 (2018), <https://onlinelibrary.wiley.com/doi/pdf/10.1002/wcms.1371>.
- ⁸³H.-J. Werner, P. J. Knowles, F. R. Manby, J. A. Black, K. Doll, A. Heßmann, D. Kats, A. Köhn, T. Korona, D. A. Kreplin, Q. Ma, T. F. Miller, A. Mitrushchenkov, K. A. Peterson, I. Polyak, G. Rauhut, and M. Sibaev, “The molpro quantum chemistry package,” *J. Chem. Phys.* **152**, 144107 (2020), <https://doi.org/10.1063/5.0005081>.
- ⁸⁴J. K. Laerdahl and P. Schwerdtfeger, “Fully relativistic *ab initio* calculation of the energies of chiral molecules including parity-violating weak interactions,” *Phys. Rev. A* **60**, 4439–4453 (1999).
- ⁸⁵P. A. M. Dirac, “Note on exchange phenomena in the Thomas atom,” *Proc. Cambridge Phil. Soc.* **26**, 376–385 (1930).
- ⁸⁶S. H. Vosko, L. Wilk, and M. Nuisar, “Accurate spin-dependent electron liquid correlation energies for local spin density calculations: A critical analysis,” *Can. J. Phys.* **58**, 1200–1211 (1980).
- ⁸⁷K. Gaul, M. G. Kozlov, T. A. Isaev, and R. Berger, “Chiral molecules as sensitive probes for direct detection of \mathcal{P} -odd cosmic fields,” *Phys. Rev. Lett.* **125**, 123004 (2020), [arXiv:2005.02429 \[hep-ph\]](https://arxiv.org/abs/2005.02429).
- ⁸⁸K. Gaul, M. G. Kozlov, T. A. Isaev, and R. Berger, “Parity nonconserving interactions of electrons in chiral molecules with cosmic fields,” *Phys. Rev. A* **102**, 032816 (2020), [arXiv:2005.03938 \[physics.chem-ph\]](https://arxiv.org/abs/2005.03938).
- ⁸⁹K. Gaul and R. Berger, “Quasi-relativistic study of nuclear electric quadrupole coupling constants in chiral molecules containing heavy elements,” *Molecular Physics* **0**, e1797199 (2020), <https://doi.org/10.1080/00268976.2020.1797199>.
- ⁹⁰G. Rauhut, V. Barone, and P. Schwerdtfeger, “Vibrational analyses for CHFClBr and CDFClBr based on high level *ab initio* calculations,” *J. Chem. Phys.* **125**, 054308 (2006), <https://doi.org/10.1063/1.2236112>.
- ⁹¹R. F. Garcia Ruiz, R. Berger, J. Billowes, C. L. Binnersley, M. L. Bissell, A. A. Breier, A. J. Brinson, K. Chrysalidis, T. E. Cocolios, B. S. Cooper, K. T. Flanagan, T. F. Giesen, R. P. de Groot, S. Franchoo, F. P. Gustafsson, T. A. Isaev, Á. Koszorus, G. Neyens, H. A. Perrett, C. M. Ricketts, S. Rothe, L. Schweikhard, A. R. Vernon, K. D. A. Wendt, F. Wienholtz, S. G. Wilkins, and X. F. Yang, “Spectroscopy of short-lived radioactive molecules,” *Nature* **581**, 396–400 (2020).

Supporting Information for

Quasi-relativistic approach to analytical gradients of parity violating potentials

Sascha A Brück,¹ Nityananda Sahu,² Konstantin Gaul,² and Robert Berger^{1,2,3,*}

¹Frankfurt Institute for Advanced Studies, Ruth-Moufang-Straße 1, 60438 Frankfurt am Main, Germany

²Fachbereich Chemie, Philipps-Universität Marburg, Hans-Meerwein-Straße 4, 35032 Marburg, Germany

³Clemens-Schöpf-Institut, Technische Universität, Darmstadt, Alarich-Weiss-Straße 4, 64287, Darmstadt, Germany

Herein, we report analytically determined Cartesian gradient components of the parity violating potential as obtained on the Hartree-Fock (HF) and local density approximation (LDA) level at the equilibrium structures of the (*S*)-enantiomer of the various methane derivatives (see Tables S1–S4). They refer to the specific equilibrium structures and orientation as reported previously in the Supplementary Material to R. Berger and J. L. Stuber, *Mol. Phys.* **105**, 41 (2007). Based on the calculations and verifications on the convergence of parity violating energies and parity violating energy gradients of few planar molecules¹, we here give the values up to four digits after the decimal point. The parity violating energy at the equilibrium structures as obtained on the HF and LDA levels are given in table S5. Molecular orbitals (MOs) have been converged until the change of the SCF energy and relative change of spin-orbit energy between two successive iterations dropped below at least $10^{-6} E_h$ and 10^{-12} respectively. MOs of CHCIF1 at the HF level, however, have been converged until the relative change of the spin-orbit energy was on the level of about 10^{-15} as the corresponding PV energy for the equilibrium structure did not achieve the desired accuracy with the 10^{-12} criterion. In practice, the spin-orbit energy criterion was by far the more restrictive one. At the end of the process, the change in SCF energy typically remained below $10^{-9} E_h$.

In table S6, we repeat unscaled harmonic vibrational wavenumbers of all normal modes as computed in R. Berger and J. L. Stuber, *Mol. Phys.* **105**, 41 (2007), but give for precision reasons one more digit. The Cartesian displacement coordinates of each of these modes, corresponding to a unit shift along the dimensionless reduced normal coordinates q_i , are given in tables S8–S11. The displacements refer to the same equilibrium structure and orientation as given in the Supplementary Material to R. Berger and J. L. Stuber, *Mol. Phys.* **105**, 41 (2007), where the displacements for q_4 were given. The various displacements are provided herein to clarify also their phase used in determining cuts through the parity violating potentials along the normal modes. Table S7 depicts the unscaled harmonic vibrational wavenumbers as computed from the anharmonic force field calculations at the CCSD(T) level of theory for the equilibrium structure of the (*S*)-enantiomer of CHBrCIF, CHCIF1, CHBrFI and CHAtFI molecules using the MOLPRO, which are utilized for calculating vibrationally averaged HF and LDA parity violating potential for energy levels.

In tables S12–S15, we give the semi-diagonal cubic force constants as computed with the SURF module of the program package Molpro. Signs have been adjusted where necessary to reflect the same phases of the normal modes as reported in tables S8–S11.

In table S16, HF and LDA level parity violating energies along the dimensionless reduced normal coordinates q

¹We are particularly grateful to Dr. Yunlong Xiao, who proposed this crucial test of the gradient to us.

ranging from -3.00 to $+3.00$ for all (except C-F stretching mode ν_4) the normal modes of the (*S*)-enantiomer of CHBrCIF are given. See the Supplementary Material to R. Berger and J. L. Stuber, *Mol. Phys.* **105**, 41 (2007) for the parity violating energies of the C-F stretching mode. The values are reported up to four digits after the decimal point.

Tables S17–S20 depict the HF and LDA level PV energy gradients along the dimensionless reduced normal coordinates (q_4 in the range from -3.00 to $+3.00$) corresponding to the C-F stretching mode (ν_4) for the (*S*)-enantiomers of CHBrCIF, CHClFI, CHBrFI and CHAtFI respectively. On the other hand, the HF and LDA level PV energy gradients along the dimensionless reduced normal coordinates $q = -0.125, +0.00$ and $+0.125$ corresponding to all (except C-F stretching mode ν_4) the normal modes of the (*S*)-enantiomer of CHBrCIF and CHAtFI are given respectively in tables S21 and S22. The values are reported up to four digits after the decimal point.

In table S23, the fitting coefficients of the LDA PV energy and the LDA PV energy gradients along the C-F stretching mode (ν_4) of the methane derivatives are given. Whereas in table S24, the second order derivative terms of the HF and PV LDA energy are given. These are obtained from a linear fit of the PV energy gradients at $q = -0.125, +0.00$ and $+0.125$ along the C-F stretching mode.

In tables S25 and S26, the vibrationally averaged HF and LDA parity violating potential $E_{v,PV}^S$ up to four lowest vibrational energy levels as obtained from the 1-dimensional and 2-dimensional perturbative treatment are given for all (except C-F stretching vibration ν_4) the normal modes of (*S*)-enantiomers of CHBrCIF and CHAtFI molecules. The frequency shift for the fundamental transition for all the vibrational modes are calculated. The percentage of the multimode effects in each of the energy levels are also included.

Table S1: Cartesian HF and LDA PV gradients [in Hartree/Bohr (E_h/a_0)] for the equilibrium structure of the (*S*)-enantiomer of CHBrCIF.

HF			
Atom	<i>x</i>	<i>y</i>	<i>z</i>
C	-3.8842×10^{-17}	2.1244×10^{-18}	6.0044×10^{-18}
H	1.9478×10^{-17}	-1.9051×10^{-17}	2.3026×10^{-19}
F	1.1306×10^{-17}	4.4916×10^{-17}	3.2903×10^{-18}
Cl	3.0118×10^{-17}	-2.8462×10^{-17}	-1.3334×10^{-17}
Br	-2.2059×10^{-17}	4.7270×10^{-19}	3.8093×10^{-18}
LDA			
Atom	<i>x</i>	<i>y</i>	<i>z</i>
C	-3.6279×10^{-17}	-6.2446×10^{-18}	3.0018×10^{-18}
H	1.5922×10^{-17}	-2.5747×10^{-17}	-2.3510×10^{-18}
F	1.8744×10^{-17}	7.8775×10^{-17}	4.0870×10^{-18}
Cl	4.5618×10^{-17}	-4.3166×10^{-17}	-1.4709×10^{-17}
Br	-4.4005×10^{-17}	-3.6182×10^{-18}	9.9716×10^{-18}

Table S2: Cartesian HF and LDA PV gradients [in Hartree/Bohr (E_h/a_0)] for the equilibrium structure of the (*S*)-enantiomer of CHCIFl.

HF			
Atom	<i>x</i>	<i>y</i>	<i>z</i>
C	-2.7893×10^{-16}	7.2970×10^{-17}	5.6183×10^{-17}
H	1.0442×10^{-16}	-6.9495×10^{-17}	8.5312×10^{-18}
F	9.3100×10^{-17}	2.2271×10^{-16}	-8.5350×10^{-18}
Cl	1.8676×10^{-16}	-2.3666×10^{-16}	-4.7349×10^{-17}
I	-1.0534×10^{-16}	1.0475×10^{-17}	-8.8299×10^{-18}
LDA			
Atom	<i>x</i>	<i>y</i>	<i>z</i>
C	-2.1427×10^{-16}	1.0065×10^{-18}	2.7223×10^{-17}
H	7.4268×10^{-17}	-1.0721×10^{-16}	-2.2634×10^{-17}
F	1.0395×10^{-16}	3.3577×10^{-16}	1.5177×10^{-17}
Cl	2.0673×10^{-16}	-2.2691×10^{-16}	-5.4238×10^{-17}
I	-1.7067×10^{-16}	-2.6586×10^{-18}	3.4473×10^{-17}

Table S3: Cartesian HF and LDA PV gradients [in Hartree/Bohr (E_h/a_0)] for the equilibrium structure of the (*S*)-enantiomer of CHBrFI.

HF			
Atom	<i>x</i>	<i>y</i>	<i>z</i>
C	-4.9807×10^{-16}	-2.3852×10^{-16}	3.1224×10^{-16}
H	1.6392×10^{-16}	-4.8853×10^{-16}	-3.5440×10^{-17}
F	-2.1085×10^{-17}	1.3365×10^{-15}	-9.4155×10^{-17}
Br	8.3611×10^{-16}	-4.7802×10^{-16}	-3.2091×10^{-16}
I	-4.8088×10^{-16}	-1.3141×10^{-16}	1.3827×10^{-16}
LDA			
Atom	<i>x</i>	<i>y</i>	<i>z</i>
C	-4.6695×10^{-16}	-3.4662×10^{-16}	2.4992×10^{-16}
H	4.6577×10^{-17}	-6.7754×10^{-16}	-9.3715×10^{-17}
F	8.1141×10^{-17}	2.2749×10^{-15}	-9.4929×10^{-17}
Br	1.3450×10^{-15}	-8.4772×10^{-16}	-3.2790×10^{-16}
I	-1.0058×10^{-15}	-4.0300×10^{-16}	2.6663×10^{-16}

Table S4: Cartesian HF and LDA PV gradients [in Hartree/Bohr (E_h/a_0)] for the equilibrium structure of the (*S*)-enantiomer of CHAtFI.

HF			
Atom	<i>x</i>	<i>y</i>	<i>z</i>
C	-1.8346×10^{-14}	-5.5240×10^{-16}	1.1994×10^{-14}
H	7.9044×10^{-15}	-1.0630×10^{-14}	5.6506×10^{-16}
F	-2.2707×10^{-15}	3.2661×10^{-14}	-5.2363×10^{-15}
I	2.3500×10^{-14}	-1.3753×10^{-14}	-7.2283×10^{-15}
At	-1.0788×10^{-14}	-7.7251×10^{-15}	-9.4893×10^{-17}
LDA			
Atom	<i>x</i>	<i>y</i>	<i>z</i>
C	-1.3189×10^{-14}	-2.4429×10^{-15}	3.2734×10^{-15}
H	1.6402×10^{-15}	-1.2766×10^{-14}	-6.4455×10^{-16}
F	3.2789×10^{-15}	4.3394×10^{-14}	-3.8216×10^{-15}
I	2.6614×10^{-14}	-1.9463×10^{-14}	-3.5265×10^{-15}
At	-1.8345×10^{-14}	-8.7216×10^{-15}	4.7192×10^{-15}

Table S5: Parity violating energy E_{PV} [in cm^{-1}] at the CCSD(T) optimized geometry (equilibrium structure) of the (*S*)-enantiomer of chiral methane derivatives. The reported values have been recomputed in this work, but agree with the values given in the Supplementary Material to R. Berger and J. L. Stuber, Mol. Phys. **105**, 41 (2007), except for a minor deviation (1.2×10^{-14}) on the HF level for CHCIFi as explained in the main text.

Molecule	HF	LDA
CHBrCIF	-1.4536×10^{-12}	5.3401×10^{-13}
CHCIFi	-1.3723×10^{-11}	5.3568×10^{-12}
CHBrFI	-3.8486×10^{-11}	1.9358×10^{-11}
CHAtFI	-2.3141×10^{-9}	9.6542×10^{-10}

Table S6: Unscaled harmonic vibrational wavenumbers $\tilde{\omega}$ (in cm^{-1}) as computed at the CCSD(T) level of theory for the equilibrium structure of the (*S*)-enantiomer of CHBrCIF, CHCIFi, CHBrFI and CHAtFI molecules in R. Berger and J. L. Stuber, Mol. Phys. **105**, 41 (2007). Herein, we give for precision reasons one digit after the decimal point more than reported in Tables 1.2, 4.2, 3.2 and 6.2 of the Supplementary Material to R. Berger and J. L. Stuber, Mol. Phys. **105**, 41 (2007). The C–F stretching mode corresponds to mode ν_4 . These wavenumbers along with the corresponding harmonic force field data are utilized for generating displaced geometries along one dimensional cuts.

Mode	CHBrCIF	CHCIFi	CHBrFI	CHAtFI
ν_9	224.23	193.51	143.36	100.34
ν_8	309.18	269.47	267.83	237.91
ν_7	422.59	412.95	326.37	280.21
ν_6	638.36	576.35	552.26	490.61
ν_5	786.56	776.20	653.72	603.87
ν_4	1122.11	1108.20	1101.67	1091.16
ν_3	1236.37	1210.33	1180.30	1105.56
ν_2	1334.45	1327.76	1319.34	1305.15
ν_1	3170.47	3162.06	3161.29	3154.01

Table S7: Unscaled harmonic vibrational wavenumbers $\tilde{\omega}$ (in cm^{-1}) as computed from the anharmonic force field calculations at the CCSD(T) level of theory for the equilibrium structure of the (*S*)-enantiomer of CHBrCIF, CHCIFi, CHBrFI and CHAtFI molecules using the MOLPRO. These wavenumbers are utilized in calculating vibrationally averaged HF and LDA parity violating potential for energy levels.

Mode	CHBrCIF	CHCIFi	CHBrFI	CHAtFI
ν_9	222.88	192.60	142.44	100.43
ν_8	308.45	269.30	267.40	237.82
ν_7	421.52	411.97	325.42	280.43
ν_6	637.64	575.76	552.38	490.46
ν_5	785.52	775.15	652.68	603.88
ν_4	1121.55	1107.69	1100.83	1090.74
ν_3	1235.71	1210.04	1177.67	1105.91
ν_2	1333.79	1327.28	1316.83	1305.43
ν_1	3169.72	3161.39	3159.79	3153.64

Table S8: Cartesian displacements (in Å) corresponding to a unit shift along the dimensionless reduced normal coordinates for all the normal modes of the (*S*)-enantiomer of CHBrClF.

Mode	Atom	<i>x</i>	<i>y</i>	<i>z</i>
ν_9	C	-0.0236951470	0.0121369995	-0.0087080375
	H	-0.0322354154	0.0063717963	-0.0088260917
	F	-0.0235104244	0.0069300442	-0.0041925549
	Cl	0.0163653898	0.0456299712	0.0041736273
	Br	0.0024228979	-0.0238138947	0.0005967752
ν_8	C	0.0215246864	0.0049634827	-0.0044364218
	H	0.0158073895	-0.0131073106	-0.0045836435
	F	0.0265608221	0.0555400827	0.0071490103
	Cl	0.0093571217	-0.0075179212	0.0000617805
	Br	-0.0140150985	-0.0106265759	-0.0010152722
ν_7	C	-0.0217507319	-0.0088114409	0.0205479682
	H	-0.0091707683	-0.0158381686	0.0210902277
	F	-0.0374172088	0.0214384035	-0.0116551581
	Cl	0.0217087598	-0.0176323065	-0.0011468561
	Br	0.0028128843	0.0041940244	-0.0000797945
ν_6	C	-0.0204677518	-0.0287186861	-0.0467130722
	H	-0.0455763639	-0.0384435862	-0.0483095150
	F	0.0028736501	0.0060496129	0.0078769417
	Cl	0.0027155810	-0.0014139336	0.0046862569
	Br	0.0017992081	0.0040279521	0.0037471908
ν_5	C	-0.0095604597	0.0462889358	-0.0209516218
	H	-0.0210491366	0.0417292646	-0.0220444023
	F	-0.0016544127	-0.0056890009	0.0031035543
	Cl	0.0050943299	-0.0115518078	0.0067081591
	Br	-0.0001364993	-0.0010832420	-0.0002521952
ν_4	C	-0.0350799297	0.0003784503	0.0149144708
	H	-0.0265347062	0.0091576250	0.0156634792
	F	0.0225345433	0.0001640155	-0.0100171270
	Cl	0.0004680430	-0.0002860938	0.0001007929
	Br	0.0000407286	-0.0000872085	-0.0001010525
ν_3	C	-0.0000495143	-0.0136417558	-0.0024901127
	H	0.0125806925	0.1559634666	-0.0021091781
	F	-0.0009637683	0.0019117634	0.0010722579
	Cl	0.0007570909	-0.0003366187	0.0017648758
	Br	-0.0002565881	-0.0002284905	-0.0006345778
ν_2	C	0.0139161242	-0.0012544171	0.0045797156
	H	-0.1477580099	0.0120477682	0.0038286553
	F	-0.0000825568	0.0000291054	-0.0050377751
	Cl	-0.0002687167	-0.0002247786	0.0006683842
	Br	-0.0000901452	0.0001294789	0.0001713398
ν_1	C	-0.0000581460	-0.0000528993	0.0085152676
	H	0.0005730257	0.0002040558	-0.0984260016
	F	0.0000233032	0.0000057069	-0.0000485033
	Cl	-0.0000059327	0.0000185525	-0.0000314752
	Br	-0.0000014575	-0.0000041567	-0.0000122264

Table S9: Cartesian displacements (in Å) corresponding to a unit shift along the dimensionless reduced normal coordinates for all the normal modes of the (*S*)-enantiomer of CHCIFl.

Mode	Atom	x	y	z
ν_9	C	-0.0212404063	0.0199492085	-0.0090853486
	H	-0.0295188582	0.0109319755	-0.0092036033
	F	-0.0203089710	0.0111972216	-0.0033684127
	Cl	0.0197109129	0.0522134767	0.0061381660
	I	-0.0001481094	-0.0180376311	-0.0002549267
ν_8	C	0.0296818756	0.0088539676	-0.0042764455
	H	0.0210641146	-0.0074645969	-0.0044089053
	F	0.0353448555	0.0582786261	0.0107873970
	Cl	0.0055498284	-0.0073900626	-0.0003007127
	I	-0.0097949130	-0.0074665109	-0.0010927226
ν_7	C	-0.0207574042	-0.0090463514	0.0201598914
	H	-0.0080216300	-0.0161584574	0.0206862612
	F	-0.0355673584	0.0268612060	-0.0111820587
	Cl	0.0228323360	-0.0176434830	-0.0012953910
	I	0.0010596945	0.0018242147	-0.0000396167
ν_6	C	-0.0207018243	-0.0299003889	-0.0495556294
	H	-0.0506795808	-0.0489561842	-0.0509950074
	F	0.0028737576	0.0071753347	0.0088925595
	Cl	0.0029915407	-0.0012020640	0.0050328596
	I	0.0011055186	0.0024732711	0.0023729172
ν_5	C	-0.0096126701	0.0468249381	-0.0208181974
	H	-0.0211539443	0.0370008191	-0.0219739353
	F	-0.0014882621	-0.0056629015	0.0030134026
	Cl	0.0050174077	-0.0122486450	0.0065786270
	I	-0.0000827953	-0.0004986800	-0.0001208230
ν_4	C	-0.0357030151	-0.0004263954	0.0142219281
	H	-0.0226701910	0.0139784793	0.0149046739
	F	0.0229046432	0.0004550924	-0.0096654294
	Cl	0.0004879819	-0.0002871787	0.0001569501
	I	-0.0000073432	-0.0000596917	-0.0000594575
ν_3	C	-0.0001613314	-0.0133512694	-0.0048511523
	H	0.0195682941	0.1564269145	-0.0044208196
	F	-0.0016253549	0.0018734898	0.0018635742
	Cl	0.0008615416	-0.0004420261	0.0019598576
	I	-0.0001342274	-0.0001384761	-0.0003252128
ν_2	C	0.0131505071	-0.0016887122	0.0049986275
	H	-0.1478201172	0.0198353660	0.0042420419
	F	0.0002012968	0.0000063869	-0.0052420336
	Cl	-0.0002124418	-0.0002212976	0.0007432630
	I	-0.0000411662	0.0000621830	0.0000736043
ν_1	C	-0.0000578731	-0.0000753681	0.0084976492
	H	0.0005928256	0.0002245937	-0.0985860331
	F	0.0000198004	0.0000116463	-0.0000410375
	Cl	-0.0000048365	0.0000206554	-0.0000298142
	I	-0.0000008671	-0.0000020921	-0.0000062381

Table S10: Cartesian displacements (in Å) corresponding to a unit shift along the dimensionless reduced normal coordinates for all the normal modes of the (*S*)-enantiomer of CHBrFI.

Mode	Atom	<i>x</i>	<i>y</i>	<i>z</i>
<i>v</i> ₉	C	0.0252210102	-0.0081164111	0.0103067250
	H	0.0326015084	-0.0051137294	0.0103866888
	F	0.0239053551	-0.0044202716	0.0043240643
	Br	-0.0076555727	-0.0393145903	-0.0026691476
	I	-0.0014618339	0.0259193115	-0.0000445572
<i>v</i> ₈	C	0.0196740909	0.0127328864	-0.0037806426
	H	0.0126686453	-0.0059926238	-0.0038421466
	F	0.0240814368	0.0659518640	0.0081220619
	Br	0.0060997564	-0.0053594406	0.0004150514
	I	-0.0093596895	-0.0076971927	-0.0010860596
<i>v</i> ₇	C	0.0366416247	-0.0023428777	-0.0140064313
	H	0.0225974872	0.0049967733	-0.0142981862
	F	0.0487085811	-0.0236950216	0.0143266957
	Br	-0.0126376213	0.0108898991	-0.0007024870
	I	-0.0030773657	-0.0030430686	-0.0002699587
<i>v</i> ₆	C	0.0231049368	0.0128727133	0.0573958444
	H	0.0590454967	0.0230939771	0.0591514984
	F	-0.0043967409	-0.0029855215	-0.0106851815
	Br	-0.0014211361	0.0021842479	-0.0030830013
	I	-0.0011117563	-0.0023120845	-0.0023802769
<i>v</i> ₅	C	-0.0047566857	0.0588596220	-0.0105205363
	H	-0.0098449476	0.0569860348	-0.0110406418
	F	0.0010673899	-0.0107078916	0.0016564301
	Br	0.0012581799	-0.0045481104	0.0024967356
	I	-0.0004142612	-0.0015869577	-0.0007181555
<i>v</i> ₄	C	-0.0355805786	-0.0008124577	0.0147539179
	H	-0.0209277779	0.0047231298	0.0154297507
	F	0.0232806577	0.0002803673	-0.0097029087
	Br	0.0000661550	0.0000577165	-0.0000422751
	I	0.0000042750	-0.0000385502	-0.0000387828
<i>v</i> ₃	C	-0.0002207449	-0.0134182504	-0.0022986074
	H	0.0071296253	0.1609709288	-0.0023310393
	F	-0.0006005751	0.0018864492	0.0007729801
	Br	0.0003391174	-0.0002580776	0.0007731425
	I	-0.0001567302	-0.0001314794	-0.0003606602
<i>v</i> ₂	C	0.0127900952	-0.0004634496	0.0057629219
	H	-0.1494682381	0.0078811713	0.0048312972
	F	0.0003529074	-0.0000195203	-0.0055191868
	Br	-0.0000617102	-0.0001209125	0.0002384229
	I	-0.0000368571	0.0000593503	0.0000946852
<i>v</i> ₁	C	-0.0000641177	-0.0000210670	0.0084897660
	H	0.0006689137	-0.0000288032	-0.0986075181
	F	0.0000222592	0.0000059831	-0.0000379301
	Br	-0.0000020040	0.0000072846	-0.0000122954
	I	-0.0000013355	-0.0000032051	-0.0000063564

Table S11: Cartesian displacements (in Å) corresponding to a unit shift along the dimensionless reduced normal coordinates for all the normal modes of the (*S*)-enantiomer of CHAtFI.

Mode	Atom	<i>x</i>	<i>y</i>	<i>z</i>
<i>v</i> ₉	C	0.0266233549	-0.0069932752	0.0111689178
	H	0.0332310722	-0.0051860255	0.0111990872
	F	0.0247007571	-0.0049217068	0.0046691440
	I	-0.0038895916	-0.0383979520	-0.0006485078
	At	-0.0015651225	0.0240746465	-0.0007225401
<i>v</i> ₈	C	0.0226677518	0.0169298855	-0.0052820358
	H	0.0146791658	-0.0023822828	-0.0053489364
	F	0.0271647016	0.0722494002	0.0074145024
	I	0.0036672971	-0.0032090604	0.0004430506
	At	-0.0060397724	-0.0055534350	-0.0006110459
<i>v</i> ₇	C	-0.0424737299	0.0053931873	0.0122135326
	H	-0.0259596898	-0.0026013704	0.0123476460
	F	-0.0537882108	0.0283347896	-0.0168441066
	I	0.0091620633	-0.0078444073	0.0010118288
	At	0.0018813924	0.0018812874	0.0001552619
<i>v</i> ₆	C	0.0242887442	0.0114222854	0.0616510669
	H	0.0676705934	0.0193911426	0.0633567616
	F	-0.0048330981	-0.0022062847	-0.0121365522
	I	-0.0009825309	0.0016584086	-0.0021554098
	At	-0.0006817577	-0.0015484146	-0.0014266010
<i>v</i> ₅	C	-0.0036518357	0.0620893140	-0.0092640116
	H	-0.0100282089	0.0620934260	-0.0097122176
	F	0.0008238230	-0.0116676241	0.0017969964
	I	0.0008113156	-0.0026750283	0.0014999561
	At	-0.0003080136	-0.0011739895	-0.0004930242
<i>v</i> ₄	C	-0.0344882683	-0.0045274544	0.0130794042
	H	-0.0130998469	0.0539402097	0.0138560935
	F	0.0223988699	0.0007556002	-0.0088266869
	I	0.0000749075	-0.0000201182	0.0001162955
	At	-0.0000380356	-0.0000563607	-0.0000856355
<i>v</i> ₃	C	-0.0099191450	0.0131203429	0.0063835206
	H	-0.0189718874	-0.1571545648	0.0062184214
	F	0.0075394215	-0.0018656000	-0.0038404212
	I	-0.0001926328	0.0001460040	-0.0004186315
	At	0.0000921880	0.0000850321	0.0002058081
<i>v</i> ₂	C	0.0123507661	-0.0011859941	0.0066340299
	H	-0.1496771513	0.0140968938	0.0056730542
	F	0.0004938261	0.0000931605	-0.0057932150
	I	-0.0000192636	-0.0000531357	0.0001359464
	At	-0.0000204687	0.0000238003	0.0000356421
<i>v</i> ₁	C	-0.0000694028	-0.0000357173	0.0084745120
	H	0.0007047366	0.0001657833	-0.0987465230
	F	0.0000305779	0.0000061370	-0.0000322123
	I	-0.0000019069	0.0000052481	-0.0000064353
	At	-0.0000010303	-0.0000024813	-0.0000035540

Table S12: Anharmonic potential parameters $\frac{\sqrt{h^3 c^3 \phi_i^2 \phi_j / E_h^3}}{N} \frac{\partial^3 V_{BO}}{\partial q_i^2 \partial q_j}$ (in $10^{-10} E_h$ where $N = 2$ for $i \neq j$ and $N = 6$ for $i = j$) for all normal modes in the (S)-enantiomer of CHBrCIF molecule. Values are determined by the SURF module of MOLPRO package.

$i \downarrow j \rightarrow$	9	8	7	6	5	4	3	2	1
9	-6.13375	-1.62456	5.36623	4.10039	-12.4538	4.22933	0.50045	-11.9076	7.06316
8	0.71152	-17.6720	23.0462	25.7329	-17.7983	44.9737	15.6896	17.7276	-10.3145
7	0.42873	19.7941	29.2981	14.9578	53.7267	10.6989	-18.7207	-1.45219	-1.31528
6	-55.4164	-85.0839	60.0186	108.029	-231.883	241.612	-129.507	84.6826	-77.9350
5	-47.6829	27.0592	235.059	215.617	339.614	430.106	27.0377	-85.5338	-36.1604
4	24.8567	-38.8926	130.756	-66.9905	111.865	-1249.16	171.079	289.211	-102.387
3	40.0876	-54.2464	85.5867	612.840	268.704	58.6542	11.0916	124.468	-8633.10
2	-42.2623	18.0845	-86.3162	245.746	247.044	-917.066	152.883	-220.018	-7319.62
1	20.8170	56.0084	-137.426	79.3191	116.667	-3.22304	-319.689	545.220	25965.9

Table S13: Anharmonic potential parameters $\frac{\sqrt{h^3 c^3 \phi_i^2 \phi_j / E_h^3}}{N} \frac{\partial^3 V_{BO}}{\partial q_i^2 \partial q_j}$ (in $10^{-10} E_h$ where $N = 2$ for $i \neq j$ and $N = 6$ for $i = j$) for all normal modes in the (S)-enantiomer of CHClFI molecule. Values are determined by the SURF module of MOLPRO package.

$i \downarrow j \rightarrow$	9	8	7	6	5	4	3	2	1
9	-4.19337	-1.70009	2.61317	5.11825	-13.0533	5.23462	-1.60110	-10.7496	3.98759
8	-3.46222	-12.6386	5.42075	19.4367	-21.3291	40.8662	11.9068	17.2613	-5.85553
7	3.68053	15.5899	30.3290	10.9146	55.8242	14.3710	-22.3170	3.34165	0.43056
6	-44.3359	-60.0953	35.7051	74.1749	-192.347	238.719	-138.832	82.7481	-174.690
5	-36.2867	7.93016	226.964	169.990	344.654	423.203	24.4129	-89.5973	-62.1807
4	14.6965	-27.2956	116.342	-35.8603	83.2129	-1221.51	275.218	258.731	-185.571
3	27.1614	-54.9990	86.3211	537.408	242.523	52.8710	70.1948	68.1178	-8661.77
2	-30.3118	20.4339	-95.2055	201.466	279.917	-876.640	269.044	-230.763	-7265.97
1	18.3341	46.2788	-133.782	61.7095	133.774	21.4595	-401.942	542.422	25887.1

Table S14: Anharmonic potential parameters $\frac{\sqrt{h^3 c^3 \theta_i^2 \theta_j / E_h^3}}{N} \frac{\partial^3 V_{B0}}{\partial q_i^2 \partial q_j}$ (in $10^{-10} E_h$ where $N = 2$ for $i \neq j$ and $N = 6$ for $i = j$) for all normal modes in the (S)-enantiomer of CHBrFI molecule. Values are determined by the SURF module of MOLPRO package.

$i \downarrow j \rightarrow$	9	8	7	6	5	4	3	2	1
9	1.79341	-0.60263	-0.86106	-0.07134	-2.08984	3.09786	-0.94865	-4.76112	8.09375
8	-0.68138	-10.1028	-19.7331	-15.5721	-16.9851	47.6269	10.6298	19.4276	-13.6836
7	3.91013	17.4723	-15.9871	-14.7202	30.7159	9.94616	-16.8515	-5.03895	-0.54352
6	27.8037	-31.2720	-32.4707	-32.3795	-93.4651	243.544	-57.4575	94.4397	-188.794
5	33.1357	-9.14426	-138.918	-305.388	101.118	333.219	29.3854	-18.0517	-21.3783
4	-9.80643	-15.9821	-74.7237	52.1214	-44.9397	-1225.40	116.039	219.153	-144.128
3	-20.2874	-34.8657	-115.646	-540.682	131.077	66.2428	52.3268	67.2387	-9110.10
2	23.9787	16.8476	59.4691	-265.576	100.108	-893.103	115.747	-249.058	-7326.72
1	-8.35726	26.8477	107.242	-137.057	71.1484	48.3217	-32.1477	597.936	25802.9

Table S15: Anharmonic potential parameters $\frac{\sqrt{h^3 c^3 \theta_i^2 \theta_j / E_h^3}}{N} \frac{\partial^3 V_{B0}}{\partial q_i^2 \partial q_j}$ (in $10^{-10} E_h$ where $N = 2$ for $i \neq j$ and $N = 6$ for $i = j$) for all normal modes in the (S)-enantiomer of CHAIFI molecule. Values are determined by the SURF module of MOLPRO package.

$i \downarrow j \rightarrow$	9	8	7	6	5	4	3	2	1
9	0.59835	-0.22248	0.17400	0.17674	-0.91244	1.81629	0.42816	-2.48089	7.30931
8	-0.32623	-7.96470	10.8695	-11.2747	-17.1353	46.6723	5.11632	20.6620	-11.3335
7	2.90929	12.4169	10.3253	-10.7379	26.1788	9.33768	17.9418	-1.44316	-6.44476
6	17.0482	-18.4112	19.0939	-16.0849	-58.0260	223.427	114.345	90.3820	-256.771
5	20.5969	-22.2024	104.276	-254.497	49.6887	324.090	78.0286	-10.8920	-16.8507
4	-2.79086	-28.2270	37.9584	-15.8978	-39.7440	-1035.41	-1080.63	207.679	-1197.41
3	-11.7552	-13.7079	98.0477	-397.161	18.6263	-239.018	-79.0787	-89.2830	-8502.01
2	13.7907	9.70384	-50.2351	-230.491	141.044	-757.859	-392.472	-291.813	-7329.56
1	-1.01056	22.9703	-52.0535	-156.455	83.2103	-19.4454	245.595	644.071	25733.2

Table S16: HF and LDA level parity violating energy (E_{pv} in 10^{-12} cm^{-1}) along the dimensionless reduced normal coordinates q ranging from -3.00 to $+3.00$ for all (except C-F stretching mode v_4) the normal modes for the (S)-enantiomer of CHBrClF.

HF^a									
$q \downarrow$	v_9	v_8	v_7	v_6	v_5	v_3	v_2	v_1	
-3.00	-0.5287	-5.5001	-4.9498	-2.5200	0.4491	2.1578	2.1779	-1.4239	
-2.50	-0.6838	-4.8322	-4.3479	-2.2988	-0.0016	1.5135	1.7398	-1.4375	
-2.00	-0.8379	-4.1631	-3.7531	-2.0979	-0.3993	0.8929	1.2216	-1.4481	
-1.50	-0.9914	-3.4918	-3.1660	-1.9149	-0.7439	0.2862	0.6331	-1.4554	
-1.00	-1.1448	-2.8172	-2.5867	-1.7477	-1.0353	-0.3070	-0.0156	-1.4594	
-0.50	-1.2986	-2.1381	-2.0157	-1.5945	-1.2722	-0.8882	-0.7143	-1.4587	
-0.25	-1.3758	-1.7966	-1.7334	-1.5223	-1.3700	-1.1729	-1.0794	-1.4565	
-0.125	-1.4146	-1.6252	-1.5931	-1.4874	-1.4135	-1.3139	-1.2653	-1.4552	
+0.125	-1.4923	-1.2811	-1.3142	-1.4193	-1.4897	-1.5911	-1.6434	-1.4510	
+0.25	-1.5313	-1.1084	-1.1757	-1.3871	-1.5222	-1.7282	-1.8352	-1.4487	
+0.50	-1.6097	-0.7615	-0.9003	-1.3227	-1.5769	-1.9973	-2.2238	-1.4430	
+1.00	-1.7682	-0.0612	-0.3571	-1.2020	-1.6405	-2.5144	-3.0180	-1.4263	
+1.50	-1.9295	0.6491	0.1756	-1.0895	-1.6422	-2.9995	-3.8296	-1.4064	
+2.00	-2.0942	1.3712	0.6971	-0.9851	-1.5794	-3.4478	-4.6540	-1.3803	
+2.50	-2.2629	2.1066	1.2065	-0.8884	-1.4504	-3.8566	-5.4886	-1.3489	
+3.00	-2.4363	2.8574	1.7028	-0.7996	-1.2534	-4.2252	-6.3323	-1.3135	
LDA^b									
$q \downarrow$	v_9	v_8	v_7	v_6	v_5	v_3	v_2	v_1	
-3.00	1.9496	-6.5506	-4.4154	-2.7572	3.9822	5.2968	3.6008	0.1024	
-2.50	1.7069	-5.4318	-3.5395	-2.0354	3.1209	4.4504	3.2743	0.1912	
-2.00	1.4673	-4.2888	-2.6844	-1.3911	2.3787	3.6381	2.8544	0.2724	
-1.50	1.2306	-3.1214	-1.8498	-0.8179	1.7520	2.8430	2.3555	0.3467	
-1.00	0.9966	-1.9291	-1.0352	-0.3098	1.2377	2.0586	1.7927	0.4147	
-0.50	0.7646	-0.7111	-0.2406	0.1391	0.8327	1.2865	1.1808	0.4770	
-0.25	0.6492	-0.0920	0.1492	0.3430	0.6703	0.9072	0.8610	0.5061	
-0.125	0.5916	0.2201	0.3423	0.4401	0.5989	0.7197	0.6983	0.5202	
+0.125	0.4765	0.8497	0.7245	0.6248	0.4755	0.3502	0.3684	0.5475	
+0.25	0.4190	1.1672	0.9137	0.7127	0.4234	0.1684	0.2015	0.5607	
+0.50	0.3041	1.8079	1.2882	0.8796	0.3381	-0.1879	-0.1350	0.5862	
+1.00	0.0740	3.1126	2.0217	1.1803	0.2410	-0.8664	-0.8147	0.6340	
+1.50	-0.1571	4.4505	2.7336	1.4398	0.2379	-1.4886	-1.4954	0.6775	
+2.00	-0.3903	5.8241	3.4230	1.6613	0.3230	-2.0437	-2.1687	0.7167	
+2.50	-0.6265	7.2364	4.0886	1.8475	0.4893	-2.5254	-2.8278	0.7518	
+3.00	-0.8667	8.6903	4.7287	2.0006	0.7287	-2.9345	-3.4667	0.7825	

^a See Fig. 5 in the manuscript.
^b See Fig. 6 in the manuscript.

Table S17: HF and LDA level PV energy gradients (in 10^{-13} cm $^{-1}$) along the dimensionless reduced normal coordinates (q_4 in the range from -3.00 to $+3.00$) corresponding to the C-F stretching mode (ν_4) for the (*S*)-enantiomer of CHBrCIF.

q_4	HF ^c	LDA ^d
-3.00	6.5348	5.9820
-2.50	6.2156	5.7207
-2.00	5.8549	5.4571
-1.50	5.4637	5.1881
-1.00	5.0524	4.9115
-0.50	4.6304	4.6259
-0.25	4.4178	4.4795
-0.125	4.3116	4.4052
+0.00	4.2055	4.3303
+0.125	4.0996	4.2547
+0.25	3.9940	4.1783
+0.50	3.7842	4.0234
+1.00	3.3717	3.7038
+1.50	2.9715	3.3695
+2.00	2.5863	3.0179
+2.50	2.2176	2.6463
+3.00	1.8659	2.2512

^c See the black curve of Fig. 1 in the manuscript.

^d See the red curve of Fig. 1 in the manuscript.

Table S18: HF and LDA level PV energy gradients (in 10^{-12} cm $^{-1}$) along the dimensionless reduced normal coordinates (q_4 in the range from -3.00 to $+3.00$) corresponding to the C-F stretching mode (ν_4) for the (*S*)-enantiomer of CHCIFl.

q_4	HF ^e	LDA ^f
-3.00	5.9614	4.0531
-2.50	5.6971	3.8461
-2.00	5.4058	3.6512
-1.50	5.0972	3.4647
-1.00	4.7792	3.2837
-0.50	4.4587	3.1057
-0.25	4.2992	3.0172
-0.125	4.2198	2.9729
+0.00	4.1407	2.9285
+0.125	4.0621	2.8841
+0.25	3.9839	2.8358
+0.50	3.8289	2.7500
+1.00	3.5253	2.5679
+1.50	3.2310	2.3798
+2.00	2.9461	2.1834
+2.50	2.6699	1.9761
+3.00	2.4011	1.7554

^e See the black curve of Fig. 2 in the manuscript.

^f See the red curve of Fig. 2 in the manuscript.

Table S19: HF and LDA level PV energy gradients (in 10^{-12} cm $^{-1}$) along the dimensionless reduced normal coordinates (q_4 in the range from -3.00 to $+3.00$) corresponding to the C-F stretching mode (ν_4) for the (*S*)-enantiomer of CHBrFI.

q_4	HF ^g	LDA ^h
-3.00	10.1319	10.3314
-2.50	9.6182	9.7016
-2.00	9.1004	9.1613
-1.50	8.5834	8.6982
-1.00	8.0720	8.3008
-0.50	7.5702	7.9578
-0.25	7.3240	7.8033
-0.125	7.2022	7.7298
+0.00	7.0813	7.6584
+0.125	6.9613	7.5890
+0.25	6.8423	7.5216
+0.50	6.6073	7.3915
+1.00	6.1497	7.1460
+1.50	5.7088	6.9103
+2.00	5.2843	6.6732
+2.50	4.8752	6.4240
+3.00	4.4800	6.1528

^g See the black curve of Fig. 3 in the manuscript.

^h See the red curve of Fig. 3 in the manuscript.

Table S20: HF and LDA level PV energy gradients (in 10^{-10} cm $^{-1}$) along the dimensionless reduced normal coordinates (q_4 in the range from -3.00 to $+3.00$) corresponding to the C-F stretching mode (ν_4) for the (*S*)-enantiomer of CHAtFI.

q_4	HF ⁱ	LDA ^j
-3.00	7.3066	5.5571
-2.50	5.7823	4.1579
-2.00	4.4400	2.9386
-1.50	3.2641	1.8925
-1.00	2.2407	1.0124
-0.50	1.3571	0.2908
-0.25	0.9641	-0.0130
-0.125	0.7792	-0.1511
+0.00	0.6017	-0.2803
+0.125	0.4317	-0.4005
+0.25	0.2687	-0.5121
+0.50	-0.0362	-0.7098
+1.00	-0.5666	-1.0083
+1.50	-0.9988	-1.1877
+2.00	-1.3414	-1.2613
+2.50	-1.6028	-1.2437
+3.00	-1.7904	-1.1509

ⁱ See the black curve of Fig. 4 in the manuscript.

^j See the red curve of Fig. 4 in the manuscript.

Table S21: HF and LDA level PV energy gradients (in 10^{-12} cm^{-1}) along the dimensionless reduced normal coordinates $q = -0.125, +0.00$ and $+0.125$ corresponding to all (except C-F stretching mode ν_4) the normal modes for the (*S*)-enantiomer of CHBrCIF.

level→	HF			LDA		
$q \rightarrow$	-0.125	+0.00	+0.125	-0.125	+0.00	+0.125
ν_9	-0.3102	-0.3109	-0.3117	-0.4606	-0.4603	-0.4599
ν_8	1.3727	1.3762	1.3798	2.5042	2.5185	2.5330
ν_7	1.1201	1.1155	1.1109	1.5391	1.5289	1.5188
ν_6	0.2764	0.2709	0.2657	0.7639	0.7389	0.7147
ν_5	-0.3340	-0.3052	-0.2764	-0.5452	-0.4934	-0.4423
ν_3	-1.1210	-1.1108	-1.0998	-1.4930	-1.4786	-1.4626
ν_2	-1.4962	-1.5124	-1.5275	-1.3081	-1.3198	-1.3301
ν_1	0.0132	0.0157	0.0183	0.1116	0.1092	0.1069

Table S22: HF and LDA level PV energy gradients (in 10^{-10} cm^{-1}) along the dimensionless reduced normal coordinates $q = -0.125, +0.00$ and $+0.125$ corresponding to all (except C-F stretching mode ν_4) the normal modes for the (*S*)-enantiomer of CHAtFI.

level→	HF			LDA		
$q \rightarrow$	-0.125	+0.00	+0.125	-0.125	+0.00	+0.125
ν_9	0.0046	0.0191	0.0339	0.4940	0.5269	0.5603
ν_8	8.9103	8.8930	8.8765	13.2760	13.3180	13.3601
ν_7	9.0001	8.9958	8.9906	8.4481	8.4193	8.3896
ν_6	2.6553	2.6699	2.6809	-1.6813	-1.7444	-1.8104
ν_5	-4.9944	-4.8033	-4.6128	-5.9296	-5.6624	-5.3986
ν_3	7.1157	7.1016	7.0713	8.4074	8.4663	8.5023
ν_2	-5.9394	-5.9911	-6.0373	-2.2852	-2.2364	-2.1833
ν_1	0.1626	0.2124	0.2623	0.3981	0.3808	0.3638

Table S23: Fitting coefficients of the LDA PV energy (E_{PV})^k and the LDA PV energy gradients ($\vec{\nabla}E_{PV}$)^l along the C-F stretching mode (ν_4) of the chiral halogenated methane derivatives in 10^{-12} cm^{-1} .

molecules		E_{PV} ^m	$\vec{\nabla}E_{PV}$	
CHBrCIF	b ₀	0.5343(2)		
	b ₁	0.4333(2)	0.433 14(5)	a ₀
	b ₂	-0.030 53(4)	-0.030 04(3)	a _{1/2}
	b ₃	-0.000 78(3)	-0.000 792(4)	a _{2/3}
CHClFI	b ₀	5.356 72(5)		
	b ₁	2.928 80(4)	2.9281(3)	a ₀
	b ₂	-0.177 41(3)	-0.177 28(2)	a _{1/2}
	b ₃	-0.000 912(7)	-0.000 89(3)	a _{2/3}
	b ₄	-0.000 774(4)	-0.000 79(1)	a _{3/4}
CHBrFI	b ₀	19.357 69(5)		
	b ₁	7.658 24(5)	7.6584(1)	a ₀
	b ₂	-0.281 38(4)	-0.2813(1)	a _{1/2}
	b ₃	0.021 587(7)	0.0216(10)	a _{2/3}
	b ₄	-0.003 719(4)	0.003 72(5)	a _{3/4}
CHAtFI	b ₀	965.44(7)		
	b ₁	-27.63(7)	-27.6(2)	a ₀
	b ₂	-49.84(5)	-49.8(1)	a _{1/2}
	b ₃	9.253(9)	9.22(2)	a _{2/3}
	b ₄	-0.335(6)	-0.338(9)	a _{3/4}

^k See Eq. 65 in the manuscript.

^l See Eq. 64 in the manuscript.

^m From Supplementary Material to R. Berger and J. L. Stuber, Mol. Phys. **105**, 41 (2007).

Table S24: Calculated values of second derivative coefficients [a_1 terms in 10^{-12} cm^{-1}] from a linear fit of the PV energy gradients at $q = -0.125, +0.00$ and $+0.125$ along the C-F stretching mode (ν_4) of the chiral methane derivatives.

molecule	HF	LDA
CHBrCIF	-0.084 80(5)	-0.060(2)
CHClFI	-0.6307(9)	-0.3551(2)
CHBrFI	-0.963(2)	-0.563(5)
CHAtFI	-139.0(2)	-100.0(2)

Table S25: Vibrationally averaged HF and LDA parity violating potential $E_{v,PV}^S$ for energy levels n in 10^{-12} cm $^{-1}$ for all (except C-F stretching vibration ν_4) the normal modes of (*S*)-enantiomer of CHBrCIF.

Mode	n	HF			LDA		
		Perturbed 1D	Perturbed 2D	2D effects (%) ^{aa}	Perturbed 1D	Perturbed 2D	2D effects (%) ^{aa}
ν_9	0	-1.4639	-1.4686	0.32	0.5218	0.5166	-1.00
	1	-1.4844	-1.4984	0.95	0.4974	0.4819	-3.11
	2	-1.5049	-1.5283	1.56	0.4730	0.4472	-5.45
	3	-1.5254	-1.5582	2.15	0.4486	0.4125	-8.05
	1 \leftarrow 0	-0.0205	-0.0299	45.67	-0.0244	-0.0347	42.24
ν_8	0	-1.3973	-1.4088	0.82	0.6529	0.6345	-2.83
	1	-1.2847	-1.3191	2.68	0.8908	0.8354	-6.22
	2	-1.1720	-1.2294	4.89	1.1286	1.0363	-8.18
	3	-1.0594	-1.1397	7.58	1.3665	1.2372	-9.46
	1 \leftarrow 0	0.1126	0.0897	-20.36	0.2379	0.2009	-15.54
ν_7	0	-1.4932	-1.5069	0.92	0.4721	0.4469	-5.34
	1	-1.5723	-1.6136	2.62	0.3484	0.2727	-21.72
	2	-1.6514	-1.7202	4.16	0.2247	0.0985	-56.15
	3	-1.7305	-1.8268	5.56	0.1009	-0.0757	-175.01
	1 \leftarrow 0	-0.0791	-0.1066	34.77	-0.1237	-0.1742	40.78
ν_6	0	-1.4739	-1.4702	-0.25	0.4585	0.4784	4.34
	1	-1.5144	-1.5033	-0.74	0.3075	0.3671	19.41
	2	-1.5550	-1.5364	-1.20	0.1564	0.2559	63.57
	3	-1.5956	-1.5695	-1.63	0.0054	0.1446	2571
	1 \leftarrow 0	-0.0406	-0.0331	-18.36	-0.1510	-0.1112	-26.34
ν_5	0	-1.3757	-1.4504	5.43	0.6697	0.5591	-16.50
	1	-1.2198	-1.4440	18.38	0.9409	0.6094	-35.23
	2	-1.0640	-1.4377	35.12	1.2122	0.6597	-45.58
	3	-0.9081	-1.4313	57.61	1.4835	0.7100	-52.14
	1 \leftarrow 0	0.1559	0.0064	-95.91	0.2713	0.0503	-81.46
ν_3	0	-1.4316	-1.4281	-0.25	0.5655	0.5669	0.25
	1	-1.3877	-1.3771	-0.77	0.6284	0.6326	0.66
	2	-1.3438	-1.3261	-1.32	0.6914	0.6984	1.00
	3	-1.2999	-1.2750	-1.91	0.7544	0.7641	1.29
	1 \leftarrow 0	0.0439	0.0510	16.11	0.0630	0.0657	4.41
ν_2	0	-1.5023	-1.4882	-0.94	0.4969	0.5100	2.64
	1	-1.5996	-1.5573	-2.65	0.4226	0.4619	9.31
	2	-1.6970	-1.6264	-4.16	0.3483	0.4139	18.84
	3	-1.7943	-1.6955	-5.51	0.2740	0.3659	33.52
	1 \leftarrow 0	-0.0973	-0.0691	-29.02	-0.0743	-0.0480	-35.33
ν_1	0	-1.4510	-1.4458	-0.36	0.5123	0.5137	0.28
	1	-1.4457	-1.4302	-1.07	0.4688	0.4730	0.92
	2	-1.4405	-1.4146	-1.79	0.4252	0.4324	1.68
	3	-1.4352	-1.3991	-2.52	0.3817	0.3918	2.63
	1 \leftarrow 0	0.0053	0.0156	196.35	-0.0435	-0.0406	-6.58

^{aa} 2D effects = (Perturbed 2D-Perturbed 1D)/Perturbed 1D

Table S26: Vibrationally averaged HF and LDA parity violating potential $E_{v,PV}^S$ for energy levels n in 10^{-12} cm $^{-1}$ for all (except C-F stretching vibration ν_4) the normal modes of (*S*)-enantiomer of CHAtFI.

Mode	n	HF			LDA		
		Perturbed 1D	Perturbed 2D	2D effects (%) ^{aa}	Perturbed 1D	Perturbed 2D	2D effects (%) ^{aa}
ν_9	0	-2311.2	-2311.8	0.03	971.00	970.95	-0.005
	1	-2305.4	-2307.3	0.08	982.15	982.01	-0.01
	2	-2299.6	-2302.8	0.14	993.30	993.07	-0.02
	3	-2293.8	-2298.3	0.20	1004.5	1004.1	-0.03
	1 \leftarrow 0	5.8	4.5	-22.16	11.15	11.06	-0.84
ν_8	0	-2289.9	-2300.7	0.47	1015.0	1002.0	-1.28
	1	-2241.7	-2274.1	1.44	1114.1	1075.0	-3.51
	2	-2193.5	-2247.4	2.46	1213.3	1148.1	-5.37
	3	-2145.3	-2220.7	3.52	1312.4	1221.2	-6.95
	1 \leftarrow 0	48.2	26.7	-44.71	99.1	73.1	-26.30
ν_7	0	-2338.9	-2348.1	0.39	937.22	920.14	-1.82
	1	-2388.5	-2416.1	1.15	880.83	829.58	-5.82
	2	-2438.2	-2484.2	1.89	824.43	739.01	-10.36
	3	-2487.9	-2552.2	2.59	768.04	648.45	-15.57
	1 \leftarrow 0	-49.7	-68.0	37.02	-56.39	-90.56	60.59
ν_6	0	-2308.8	-2314.5	0.25	950.73	946.54	-0.44
	1	-2298.2	-2315.5	0.75	921.34	908.79	-1.36
	2	-2287.6	-2316.5	1.26	891.95	871.03	-2.35
	3	-2277.1	-2317.5	1.77	862.57	833.28	-3.40
	1 \leftarrow 0	10.6	-1.0	-109.1	-29.39	-37.75	28.48
ν_5	0	-2266.9	-2286.6	0.87	1029.1	996.65	-3.16
	1	-2172.5	-2231.7	2.72	1156.6	1059.1	-8.43
	2	-2078.2	-2176.8	4.75	1284.0	1121.6	-12.65
	3	-1983.8	-2122.0	6.96	1411.5	1184.0	-16.11
	1 \leftarrow 0	94.3	54.9	-41.82	127.4	62.5	-50.99
ν_3	0	-2313.8	-2318.7	0.21	980.49	963.72	-1.71
	1	-2313.4	-2328.0	0.63	1010.6	960.32	-4.98
	2	-2312.9	-2337.3	1.06	1040.8	956.92	-8.06
	3	-2312.4	-2346.6	1.48	1070.9	953.52	-10.96
	1 \leftarrow 0	0.5	-9.3	-2075	30.1	-3.40	-111.3
ν_2	0	-2333.5	-2310.0	-1.01	972.02	986.25	1.46
	1	-2372.3	-2301.7	-2.97	985.23	1027.9	4.33
	2	-2411.1	-2293.5	-4.88	998.43	1069.6	7.13
	3	-2449.9	-2285.3	-6.72	1011.6	1111.2	9.85
	1 \leftarrow 0	-38.8	8.2	-121.2	13.20	41.7	215.5
ν_1	0	-2307.4	-2302.2	-0.22	956.05	955.73	-0.03
	1	-2294.1	-2278.6	-0.67	937.31	936.34	-0.10
	2	-2280.8	-2255.0	-1.13	918.58	916.95	-0.18
	3	-2267.5	-2231.4	-1.59	899.84	897.56	-0.25
	1 \leftarrow 0	13.3	23.6	77.49	-18.74	-19.39	3.47

^{aa} 2D effects = (Perturbed 2D-Perturbed 1D)/Perturbed 1D